

Theoretical Insights for Generation of Terminal Metal-Oxo Species: Drives for “Oxo Wall”

Monika, Aman and Azaj Ansari*

Department of Chemistry, Central University of Haryana, Mahendergarh 123031, India.

Email: ajaz.alam2@gmail.com

Computational Details

Gaussian16 program is used for all the calculations.¹ Fragment approach is present in Gaussian16, is used for all the spin state calculations. Based on previous work, it is predicted that B3LYP,² B3LYP-D2,³ wB97XD⁴ are advocated to find the correct spin as the ground state of reactant, intermediate, and product.⁵ B3LYP-D2 is most appropriate among these.⁵ So, here we have restricted our calculations only to B3LYP-D2 functional, incorporating dispersion correction of Grimme *et al.*⁶ The basis set LACVP comprises LanL2DZ-Los Alamos effective core potential for the metals (Cr, Mn, Fe, Co, Ni and Cu)⁷, and 6-31G* basis set for other atoms (hydrogen, carbon, nitrogen, and oxygen) is used.⁸ TZVP basis set is used for all atoms on the optimized geometries for the single point energy calculation.⁹ Wiberg bond indices are computed by using the natural atomic orbital analysis (NBO). NBO and SNO (spin natural orbital) are performed using G16, and the visualizations are examined by using Chemcraft software. Solvation energies are computed by the polarizable continuum model (PCM) using n,n-dimethylacetamide as a solvent. The transition state is verified by single negative frequency, animating the corresponding frequency and visualized in Gauss View. DFT energies are quoted using B3LYP-D2 solvation including free-energy corrections at 298.15 K temperature. Common notation of ${}^{\text{mult}}\text{M}_{\text{spin state}}\text{-Y}$ is used throughout, where mult denotes total multiplicity, M represents to metal (I (Cr), II (Mn), III (Fe), IV (Co), V (Ni), VI (Cu)), VII (Ru), VIII (Os), IX (Rh) and X (Ir)) and spin state denote the possible spin states and Y represents the transition state and intermediate. Here we have taken methyl group instead of *t*-butyl in buea ligand for the entire computation.

Table S1. B3LYP-D2 computed relative energies in kJ/mol.

Spin states	Energy (kJ/mol)	Spin states	Energy (kJ/mol)
[(buea)CrOOH] ⁻			[(buea)MnOOH] ⁻
⁴ I _{hs}	0.0	⁵ II _{hs}	0.0
² I _{ls}	96.2	³ II _{is}	99.2
		¹ II _{ls}	110.2
⁴ I _{hs-ts}	106.1	⁵ II _{hs-ts}	83.6
² I _{ls-ts}	90.2	³ II _{is-ts}	87.4
		¹ II _{ls-ts}	155.2
³ I _{hs-Int}	7.3	⁴ II _{hs-Int}	18.7
¹ I _{ls-Int}	124.4	² II _{ls-Int}	114.6
[(buea)FeOOH] ⁻			[(buea)CoOOH] ⁻
⁶ III _{hs}	0.0	⁵ IV _{hs}	35.4
⁴ III _{is}	60.8	³ IV _{is}	0.0
² III _{ls}	27.9	¹ IV _{ls}	40.6
⁶ III _{hs-ts}	85.2	⁵ IV _{hs-ts}	119.2
⁴ III _{is-ts}	57.7	³ IV _{is-ts}	139.8
² III _{ls-ts}	133.4		
⁵ III _{hs-Int}	44.2	⁶ IV _{hs-Int}	136.9
³ III _{is-Int}	100.6	⁴ IV _{is-Int}	118.2
¹ III _{ls-Int}	126.9	² IV _{ls-Int}	118.7
[(buea)NiOOH] ⁻			[(buea)CuOOH] ⁻
⁴ V _{hs}	0.0	³ VI _{hs}	0.00
² V _{ls}	-	¹ VI _{ls}	38.7
² V _{ls-ts}	99.8	¹ VI _{ls-ts}	154.0
⁵ V _{hs-Int}	121.5	⁴ VI _{hs-Int}	117.6
³ V _{is-Int}	132.5	² VI _{ls-Int}	133.6
¹ V _{ls-Int}	135.7		

Table S2. B3LYP-D2 computed structural parameters of the buea metal hydroperoxo species, transition states (O---O) and metal-oxo.

Spin State	Bond length (Å)										Bond Angle (°)					
	M-O	M-N ₁	M-N ₂	M-N ₃	M-N ₄	O-O	O-H ₁	O-H ₂	O-H ₃	O ₁ -M-N ₄	M-O ₁ -O ₂	N ₁ -M-N ₂	N ₂ -M-N ₃	N ₁ -M-N ₃	N ₃ -M-N ₄	O-O-H
[(buea)CrOOH] ⁻ Species																
⁴ I _{hs}	1.912	2.091	1.986	1.984	2.177	1.462	1.833	1.955	-	176.9	90.8	143.9	100.7	107.1	83.2	99.0
² I _{ls}	1.890	2.173	1.975	1.993	2.173	1.470	1.802	1.763	-	177.6	110.6	120.2	103.1	129.1	79.6	97.5
⁴ I _{hs} -ts	1.762	2.003	1.986	1.974	2.167	1.878	1.797	1.778	-	168.8	116.0	128.7	101.1	119.7	77.9	85.1
² I _{ls} -ts	1.804	1.948	1.966	1.936	2.159	1.613	1.794	1.796	1.882	172.2	120.1	114.5	115.4	120.5	79.4	95.3
³ I _{hs} -Int	1.649	1.935	1.935	1.943	2.532	-	1.947	1.929	-	179.4	179.4	116.6	115.1	109.6	75.6	-
¹ I _{ls} -Int	1.611	1.906	1.934	1.997	2.549	-	1.972	-	-	168.4	-	101.9	131.0	103.6	74.9	-
[(buea)MnOOH] ⁻ Species																
⁵ I _{hs}	1.853	2.088	2.034	2.089	2.094	1.454	1.910	0.994	-	170.8	105.4	103.8	79.9	81.3	79.1	99.6
³ I _{is}	1.858	2.008	1.936	1.933	2.129	1.466	1.970	1.918	1.776	177.2	104.4	144.3	102.14	107.7	83.9	98.5
¹ I _{ls}	1.933	1.893	1.896	1.935	2.120	1.429	1.810	1.702	1.884	178.9	110.4	115.7	112.9	125.1	80.8	98.8
⁵ I _{hs} -ts	1.732	2.006	1.994	1.988	2.126	1.856	1.833	1.891	-	176.2	125.5	131.1	101.3	118.3	79.2	86.3
³ I _{is} -ts	1.734	2.101	1.949	1.959	2.101	1.737	1.824	1.923	1.805	172.6	115.7	131.4	100.5	121.5	80.4	91.6
¹ I _{ls} -ts	1.648	1.884	1.857	2.017	2.155	1.900	1.731	1.751	1.955	161.9	127.7	117.4	102.2	128.4	75.7	85.2
⁴ I _{hs} -Int	1.674	1.928	1.986	1.952	2.236	-	1.775	1.753	-	175.9	-	137.6	113.7	100.4	82.2	-
² I _{ls} -Int	1.658	1.910	1.944	1.927	2.315	-	1.777	1.805	-	176.1	-	127.7	119.1	102.6	79.9	-
Exp. ¹⁶	1.628															
[(buea)FeOOH] ⁻ Species																
⁶ III _{hs}	1.940	1.985	1.984	2.024	2.491	1.463	1.948	1.9092	-	122.8	113.3	118.4	105.8	120.3	77.5	98.2
⁴ III _{is}	1.819	2.035	1.987	2.019	2.174	1.441	1.833	-	1.828	174.2	117.9	128.8	108.5	116.7	81.8	99.0
² III _{ls}	1.844	1.977	1.907	1.966	2.137	1.455	1.719	1.833	-	169.1	117.7	147.5	101.3	105.6	83.1	98.1
⁶ III _{hs} -ts	1.697	1.954	1.999	2.206	2.293	1.929	1.878	-	-	178.7	146.3	123.1	107.4	120.5	79.8	83.4
⁴ III _{is} -ts	1.666	1.948	2.059	1.992	2.153	1.902	1.848	-	1.822	178.5	111.3	119.4	106.1	128.9	82.5	88.2
² III _{ls} -ts	1.678	1.931	1.897	2.007	2.083	1.941	1.745	1.771	1.984	163.3	129.6	119.0	98.6	134.1	98.6	80.8
⁵ III _{hs} -Int	1.651	2.007	1.972	2.005	2.200	-	1.826	1.844	-	178.8	-	123.5	106.8	122.7	81.5	-
³ III _{is} -Int	1.661	1.885	1.934	1.960	2.227	-	1.804	1.766	-	172.1	-	141.9	111.0	98.6	81.5	-
¹ III _{ls} -Int	1.624	1.871	1.871	1.871	2.733	-	-	-	-	179.9	-	111.7	111.6	111.5	72.8	-

[(buea)CoOOH] ⁻ Species																
⁵ IV _{hs}	1.943	2.322	1.979	1.979	2.008	1.457	1.963	1.794	1.954	176.3	110.2	132.2	104.5	112.9	81.6	99.2
³ IV _{is}	1.872	2.035	2.001	2.021	1.959	1.437	1.783	1.778	-	179.5	111.8	121.2	104.3	129.9	84.4	98.5
¹ IV _{ls}	1.862	2.041	1.916	1.919	1.992	1.445	1.944	1.926	1.772	175.5	99.2	152.8	99.7	103.4	86.3	99.2
⁵ IV _{hs-ts}	1.714	1.956	1.974	1.966	2.199	1.938	1.801	1.972	-	171.3	135.2	111.9	107.1	134.1	81.8	82.6
³ IV _{is-ts}	1.724	1.953	1.930	1.928	2.235	2.015	1.751	1.823	-	173.8	137.9	130.9	118.7	103.4	80.6	84.3
⁶ IV _{hs} -Int	1.755	1.987	1.982	1.998	2.466	-	1.861	1.841	-	175.8	-	104.6	117.2	123.0	76.5	-
⁴ IV _{is} -Int	1.714	1.979	1.944	2.018	2.116	-	1.974	1.812	1.786	173.6	-	119.3	128.8	107.3	82.8	-
² IV _{ls} -Int	1.824	1.932	1.965	1.988	2.075	-	1.922	1.778	-	174.2	-	134.9	111.2	110.3	83.7	-
[(buea)NiOOH] ⁻ Species																
⁴ V _{hs}	1.969	2.405	1.968	1.945	1.972	1.457	1.929	-	1.944	169.8	113.7	114.3	114.7	121.2	79.8	99.4
² V _{ls}	1.873	2.107	2.079	1.996	1.963	1.425	-	1.842	-	169.6	115.8	108.7	105.8	142.0	83.2	100.2
² V _{ls-ts}	1.789	1.936	2.050	1.955	2.138	2.065	1.666	1.754	1.790	176.5	121.6	151.5	104.9	98.6	83.4	73.4
⁵ V _{hs} -Int	1.924	1.961	1.960	2.028	2.288	-	1.790	1.769	1.954	172.7	-	124.7	107.4	120.9	81.4	-
³ V _{is} -Int	1.972	1.959	2.015	1.954	2.262	-	1.744	1.939	1.771	172.8	-	121.4	125.7	106.7	81.9	-
¹ V _{ls} -Int	1.745	1.922	1.949	1.936	2.134	-	1.862	1.669	1.892	177.6	-	146.8	100.5	108.9	83.8	-
[(buea)CuOOH] ⁻ Species																
³ VI _{hs}	1.999	2.309	2.190	2.015	1.989	1.427	-	1.830	-	171.8	114.5	107.4	106.2	138.6	81.9	99.8
¹ VI _{ls}	1.975	2.337	2.194	1.963	1.947	1.429	-	1.975	1.001	166.6	108.3	105.5	103.7	142.5	78.5	100.3
¹ VI _{ls-ts}	1.902	2.419	1.899	1.932	2.119	1.911	1.809	-	-	132.3	92.2	112.6	99.1	85.7	83.6	97.3
⁴ VI _{hs} -Int	1.919	2.120	2.001	2.065	2.241	-	1.801	1.913	1.810	175.3	-	122.6	101.2	129.5	82.3	-
² VI _{ls} -Int	1.918	1.986	2.029	2.336	2.276	-	1.756	1.869	-	171.1	-	96.1	112.5	142.3	76.3	-

Table S3. B3LYP-D2 computed spin density values of the buea hydroperoxo species, transition states and metal-oxo.

Spin State	Metal	O ₁	O ₂
[(buea)CrOOH] ⁻ Species			
⁴ I _{hs}	3.005	-0.009	0.012
² I _{ls}	0.991	0.040	-0.009
⁴ I _{hs} -ts ² I _{ls} -ts			
	2.549	-0.024	0.545
	1.089	0.043	-0.111
³ I _{hs} -Int	1.930	0.050	-
¹ I _{ls} -Int	0	0	-
[(buea)MnOOH] ⁻ Species			
⁵ II _{hs}	3.831	-0.038	0.007
³ II _{is}	1.929	0.025	-0.012
¹ II _{ls}	0.000	0.00	0.000
⁵ II _{hs} -ts	3.301	0.056	0.577
³ II _{is} -ts	2.238	0.094	-0.312
¹ II _{ls} -ts	0.000	0.000	0.000
⁴ II _{hs} -Int	2.732	0.256	-
² II _{ls} -Int	1.004	-0.112	-
[(buea)FeOOH] ⁻ Species			
⁶ III _{hs}	3.926	0.228	0.026
⁴ III _{is}	2.771	-0.017	-0.031
² III _{ls}	0.979	0.002	-0.005
⁶ III _{hs} -ts	3.381	0.258	0.742
⁴ III _{is} -ts	2.826	0.291	-0.631
² III _{ls} -ts	1.399	0.080	-0.481
⁵ III _{hs} -Int	2.991	0.456	-
³ III _{is} -Int	1.569	0.375	-
¹ III _{ls} -Int	0	0	-
[(buea)CoOOH] ⁻ Species			
⁵ IV _{hs}	2.744	0.206	0.017
³ IV _{is}	1.719	-0.117	-0.034
¹ IV _{ls}	0.000	0.000	0.000
⁵ IV _{hs} -ts	2.107	0.526	0.506
³ IV _{is} -ts	1.423	0.279	0.553
⁶ IV _{hs} -Int	2.701	1.044	-
⁴ IV _{is} -Int	1.701	0.664	-
² IV _{ls} -Int	1.562	-0.956	-
[(buea)NiOOH] ⁻ Species			

$^4\text{V}_{\text{hs}}$	1.640	0.229	0.023
$^2\text{V}_{\text{ls}}$	0.927	-0.135	-0.052
$^2\text{V}_{\text{ls-ts}}$	0.929	0.336	0.456
$^5\text{V}_{\text{hs-Int}}$	1.615	1.104	-
$^3\text{V}_{\text{is-Int}}$	1.634	-0.808	-
$^1\text{V}_{\text{ls-Int}}$	0	0	-
[(buea)CuOOH] ⁻ Species			
$^3\text{VI}_{\text{hs}}$	0.494	0.344	0.086
$^1\text{VI}_{\text{ls}}$	0.000	0.000	0.000
$^1\text{VI}_{\text{ls-ts}}$	0	0	0
$^4\text{VI}_{\text{hs-Int}}$	0.524	1.169	-
$^2\text{VI}_{\text{ls-Int}}$	0.493	1.115	-

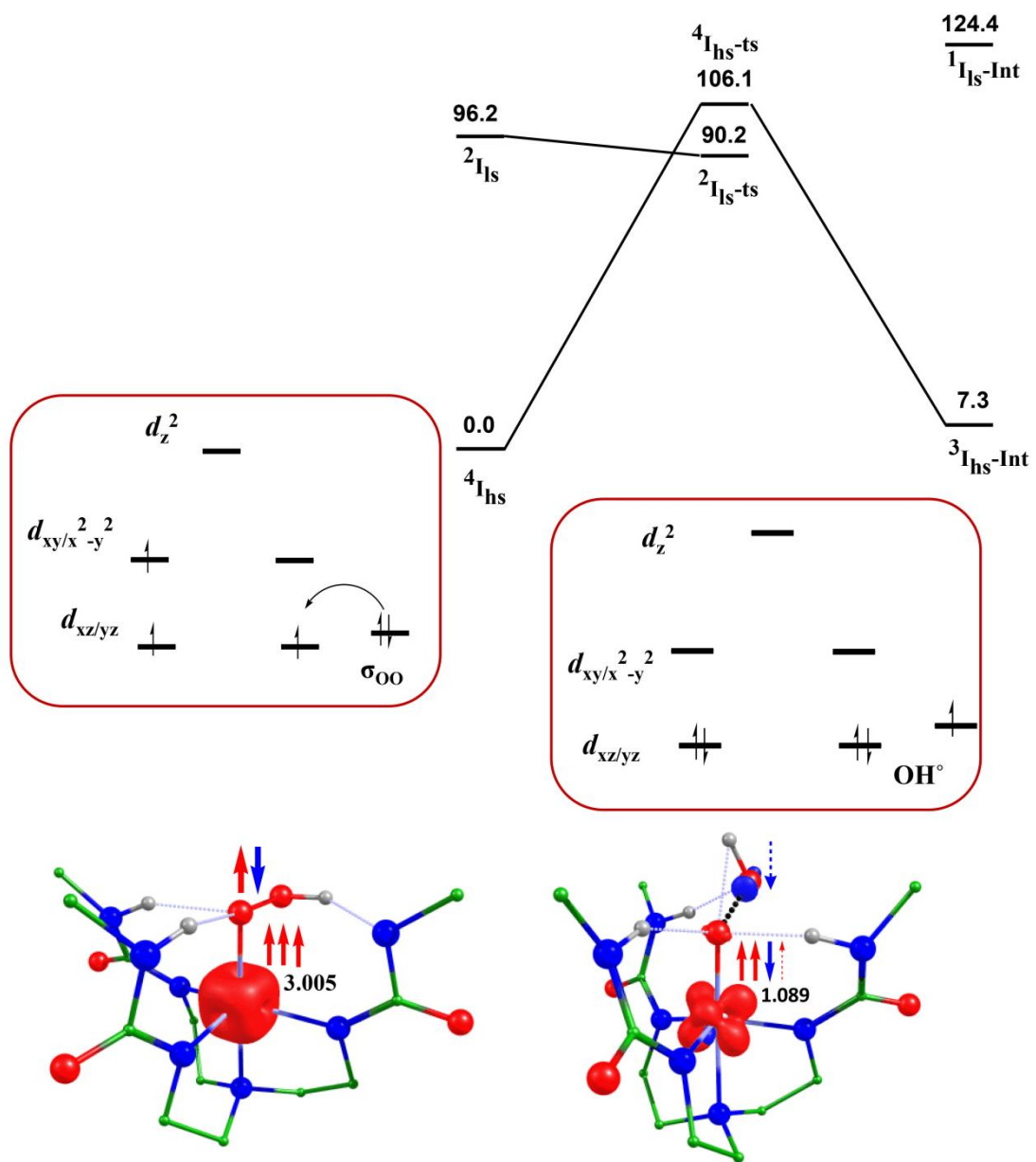


Fig. S1. B3LYP-D2 computed barrier height (ΔG in kJ mol⁻¹) along with schematic representation of electron involvement with spin density during the O-O bond cleavage of species I.

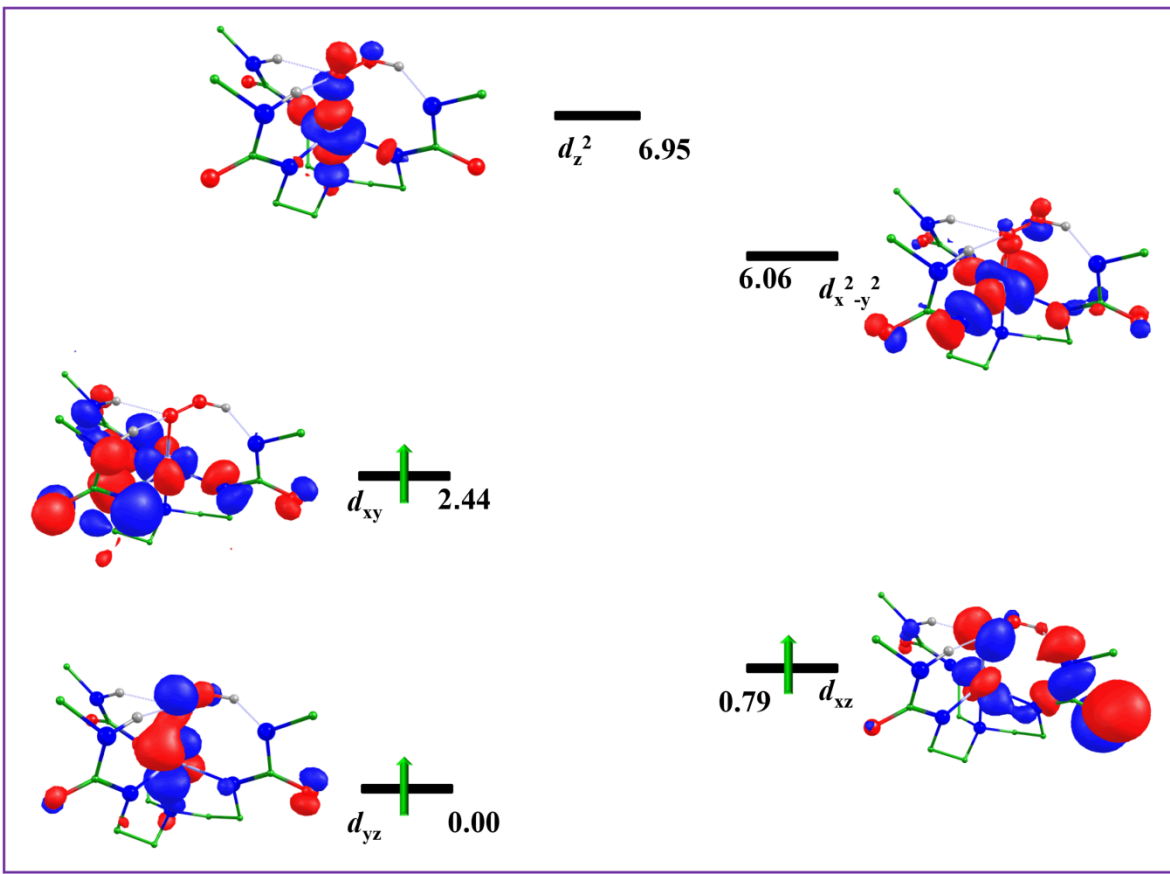


Fig. S2. Computed eigenvalue plot incorporating energies computed for *d*-based orbitals for alpha and beta spin corresponding to the ground state $^4\text{I}_{\text{hs}}$ of the species I (energies are given in eV).

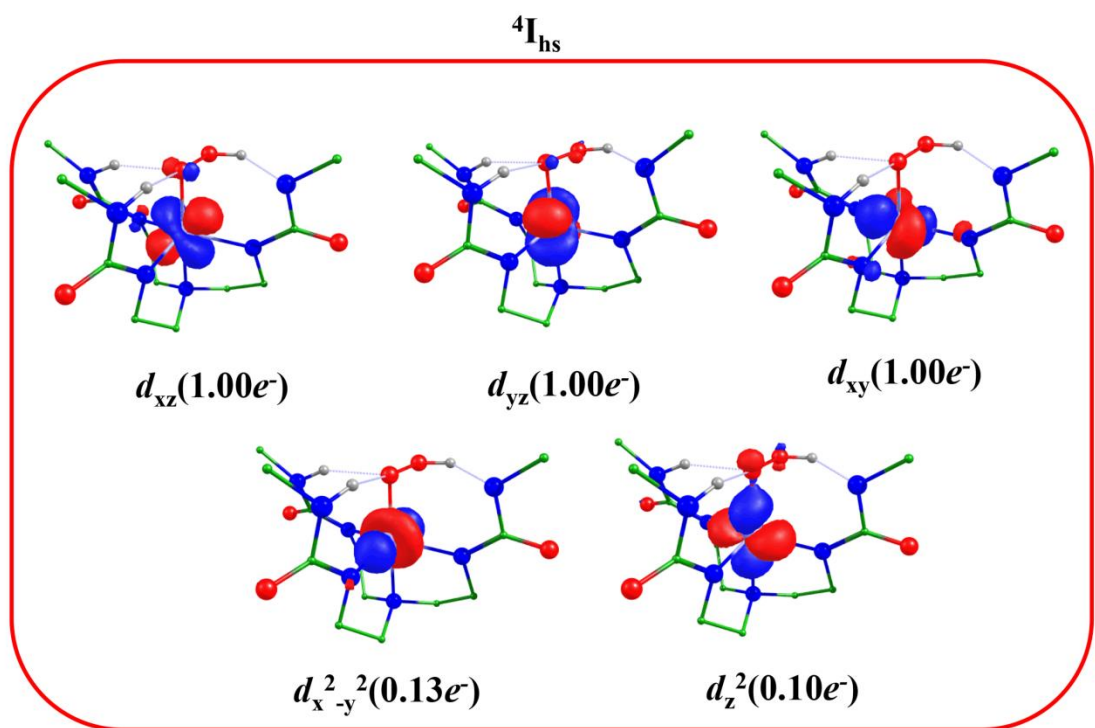


Fig. S3. Spin natural orbitals and their occupations (noted in parenthesis) of $^4\text{I}_{\text{hs}}$.

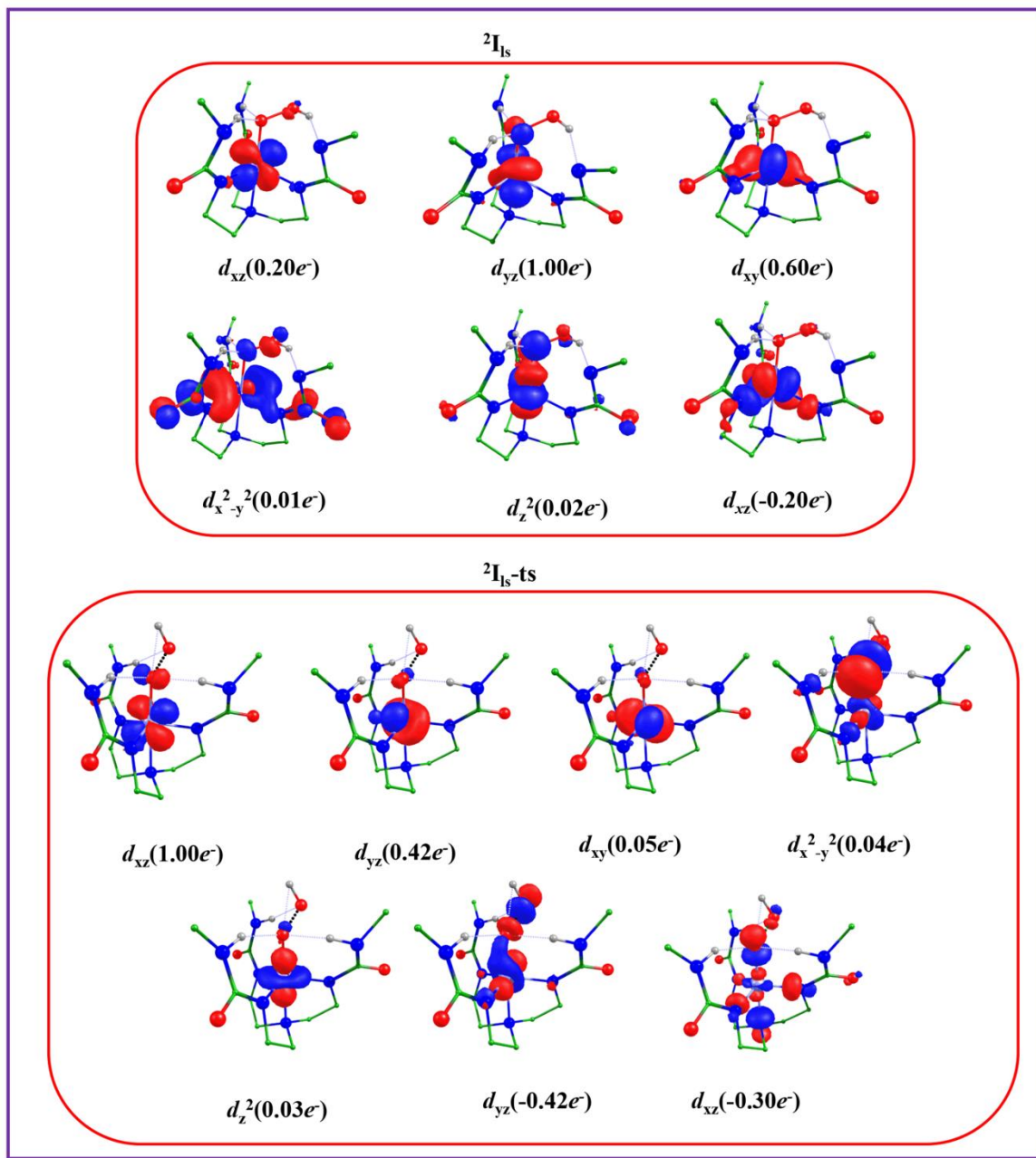


Fig. S4. Spin natural orbitals and their occupations (noted in parenthesis) of $^2\text{I}_{\text{ls}}$ and $^2\text{I}_{\text{ls-ts}}$.

Table S4. Computed Wiberg bond indices of metal species with buea ligand.

Spin State	M-O1	O1-O2
[(buea)CrOOH] ⁻ Species		
⁴ I _{hs}	0.193	0.244
² I _{ls-ts}	0.310	0.170
³ I _{hs-Int}	0.507	-
[(buea)MnOOH] ⁻ Species		
⁵ II _{hs}	0.207	0.247
⁵ II _{hs-ts}	0.339	0.201
⁴ II _{hs-Int}	0.527	-
[(buea)FeOOH] ⁻ Species		
⁶ III _{hs}	0.235	0.248
⁴ III _{is-ts}	0.528	0.044
⁵ III _{hs-Int}	0.583	-
[(buea)CoOOH] ⁻ Species		
³ IV _{is}	0.148	0.248
⁵ IV _{hs-ts}	0.388	0.215
⁴ IV _{is-Int}	0.583	-
[(buea)NiOOH] ⁻ Species		
⁴ V _{hs}	0.191	0.250
² V _{ls-ts}	0.205	0.158
⁵ V _{hs-Int}	0.226	-
[(buea)CuOOH] ⁻ Species		
³ VI _{hs}	0.165	0.272
¹ VI _{ls-ts}	0.112	0.116
⁴ VI _{hs-Int}	0.201	-

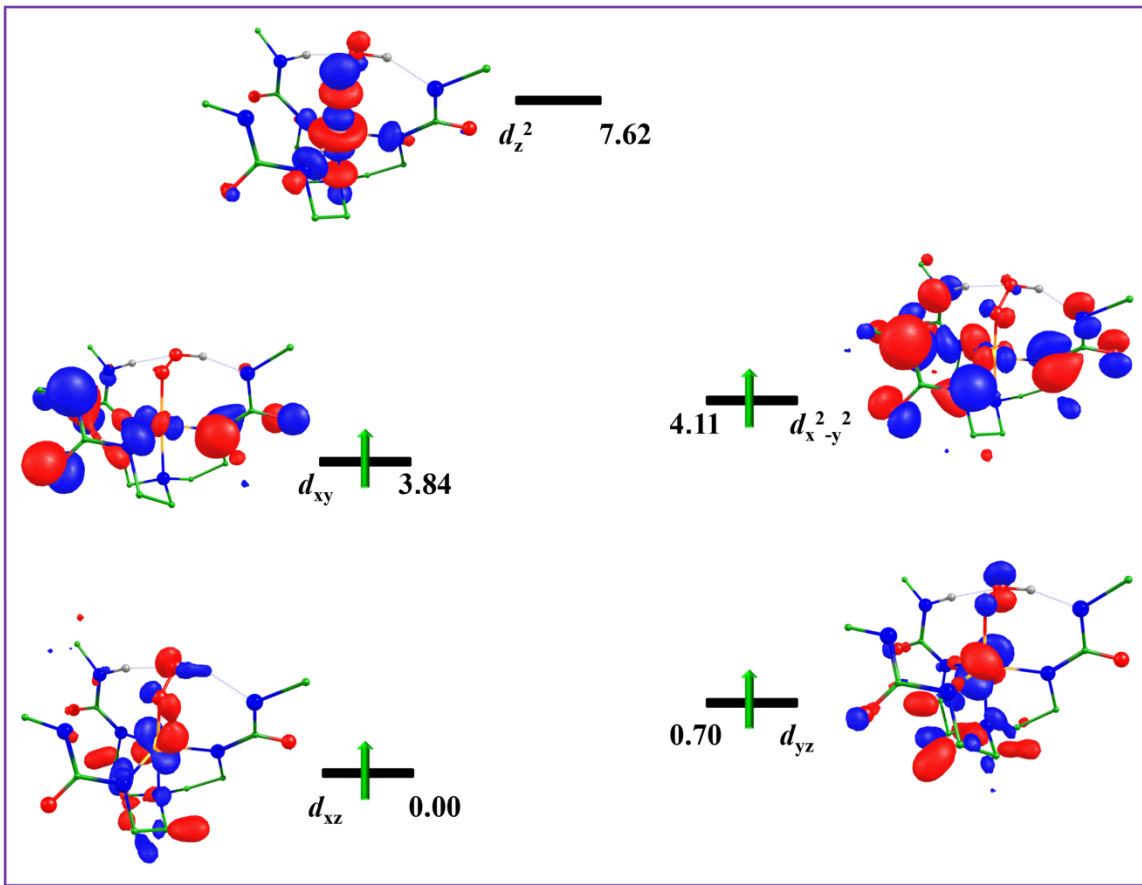


Fig. S5. Computed eigenvalue plot incorporating energies computed for d -based orbitals for alpha spin corresponding to the ground state ${}^5\text{II}_{\text{hs}}$ of the species II (energies are given in eV).

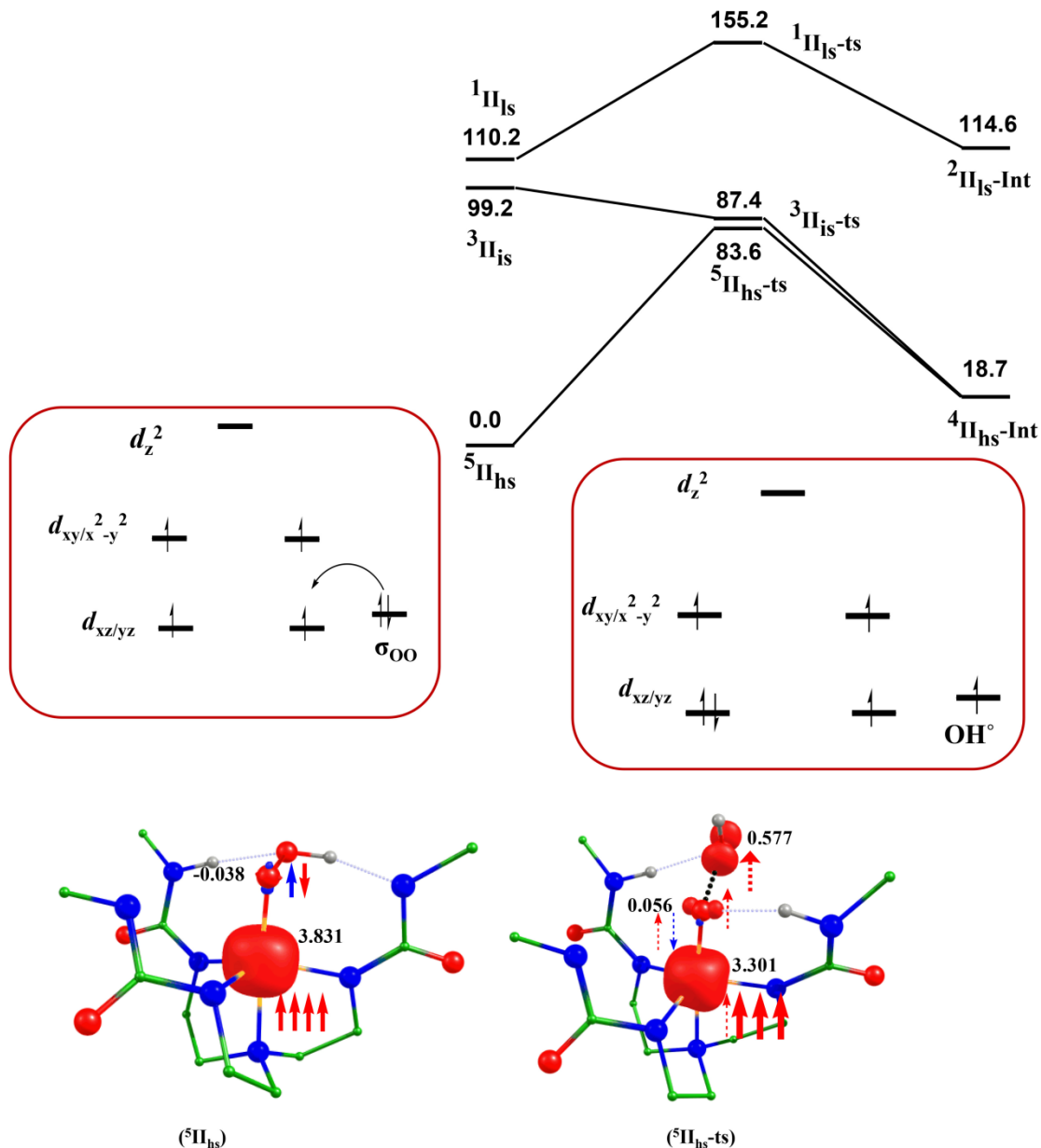


Fig. S6. B3LYP-D2 computed barrier height (ΔG in kJ mol^{-1}) along with schematic representation of electron involvement with spin density during the O--O bond cleavage of species II.

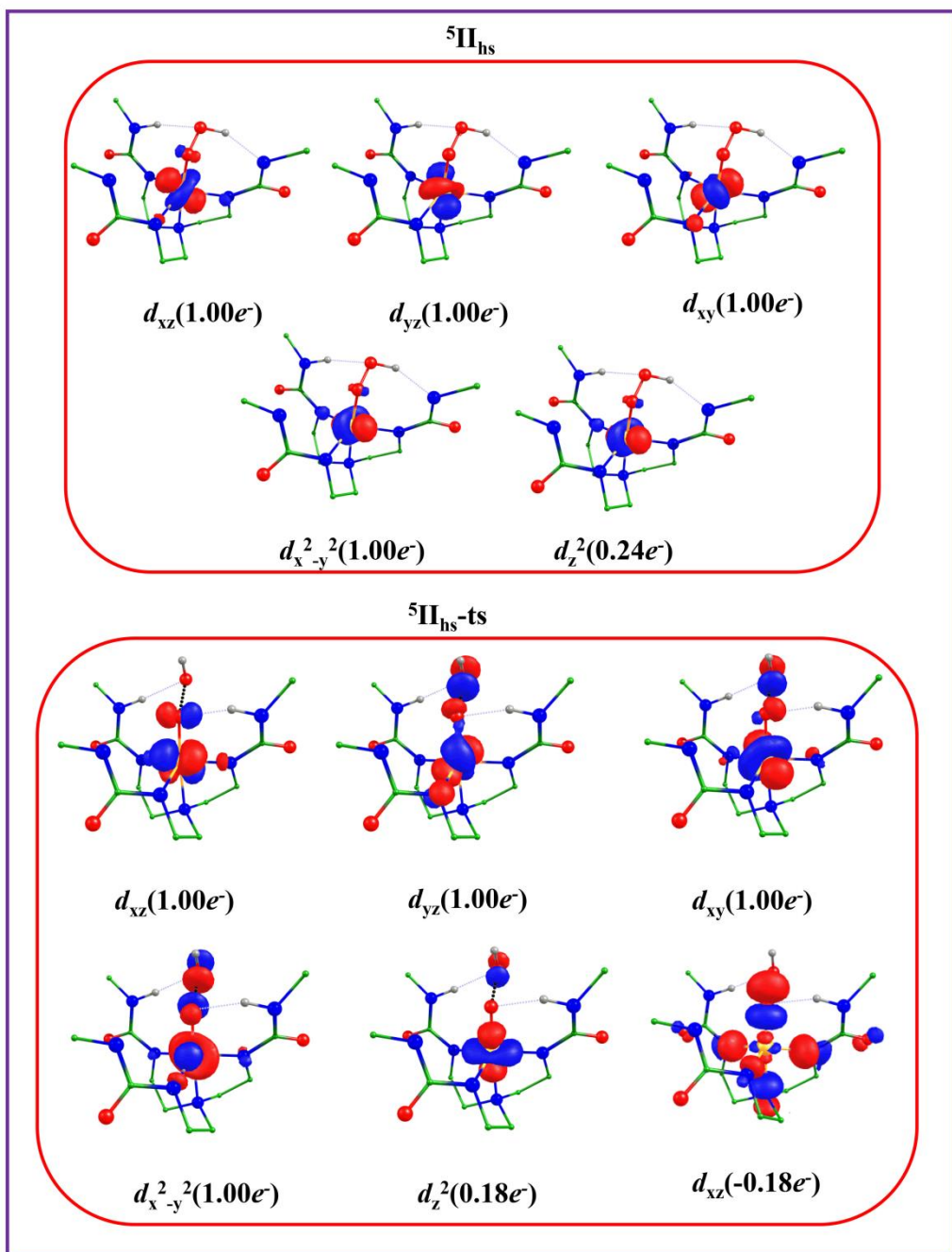


Fig. S7. Spin natural orbitals and their occupations (noted in parenthesis) of $^5\text{II}_{\text{hs}}$ and $^5\text{II}_{\text{hs-ts}}$.

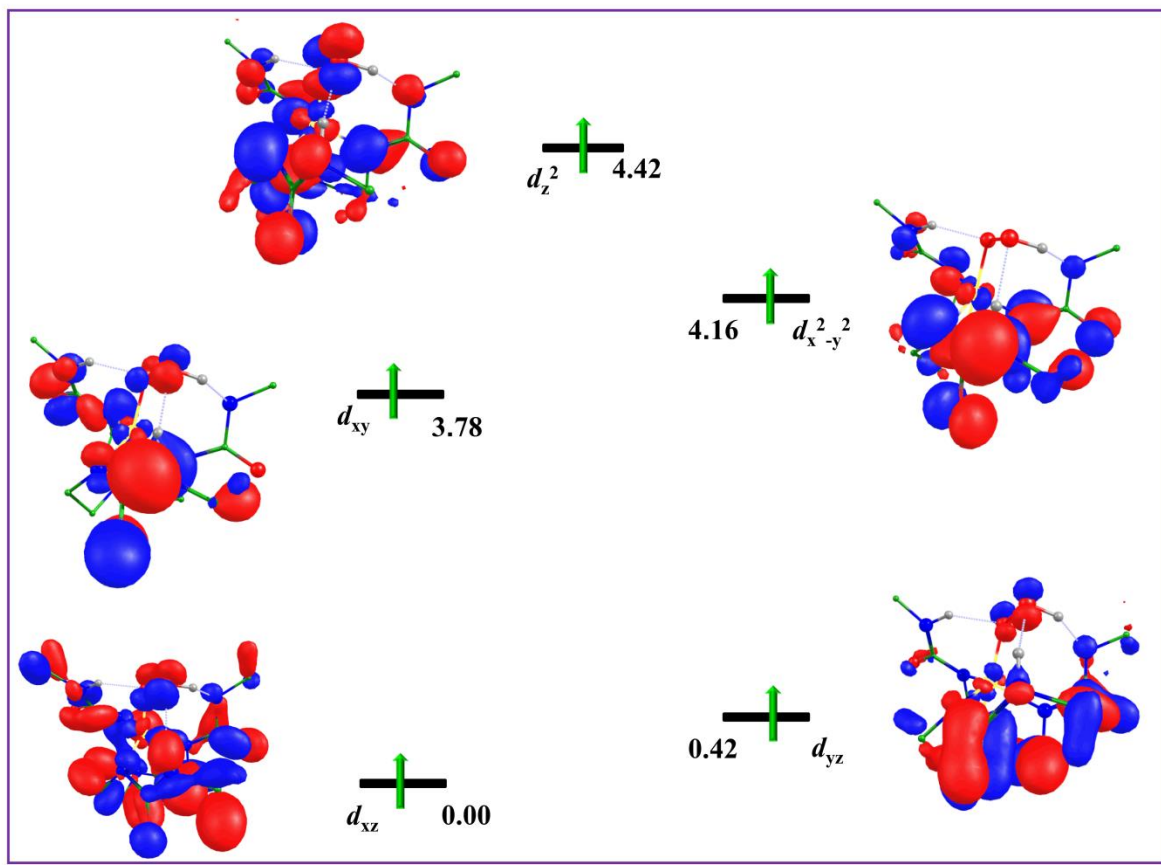


Fig. S8. Computed eigenvalue plot incorporating energies computed for d -based orbitals for alpha spin corresponding to the ground state ${}^6\text{III}_{\text{hs}}$ of the species III (energies are given in eV).

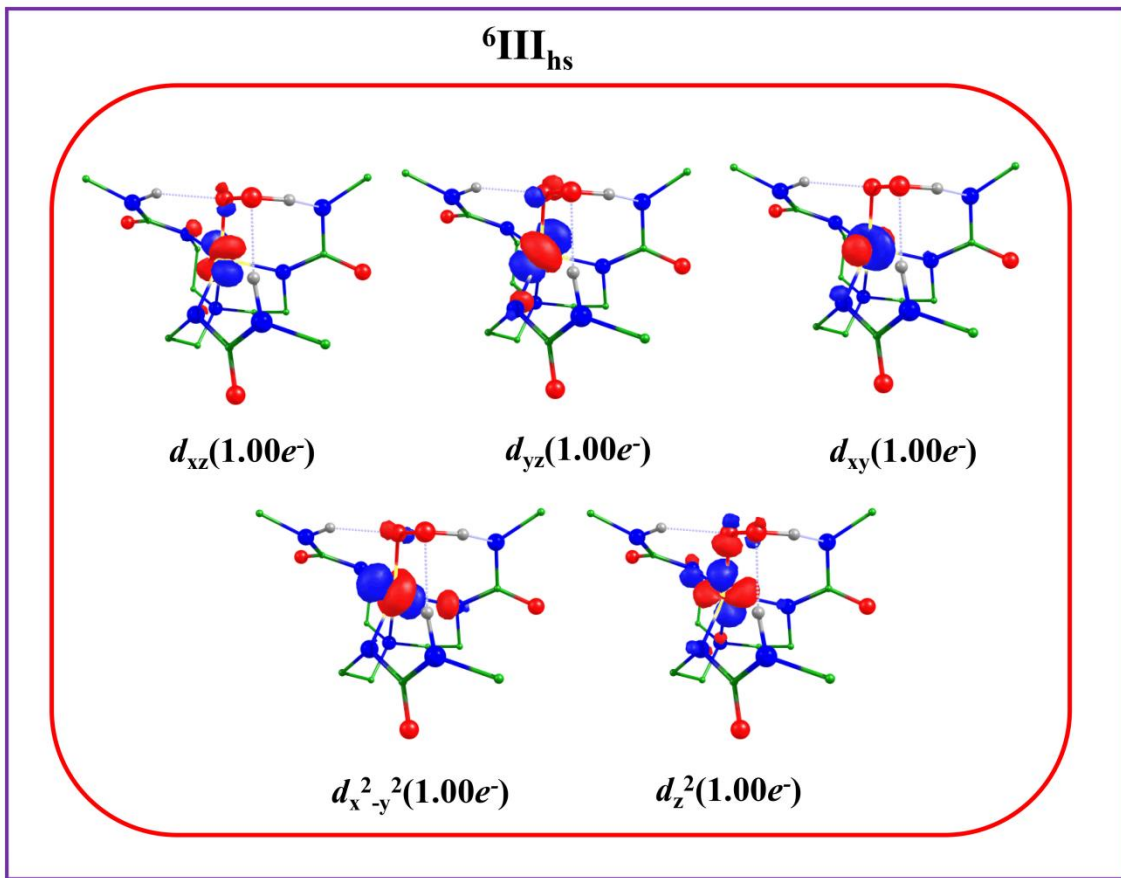


Fig. S9. Spin natural orbitals and their occupations (noted in parenthesis) of $^6\text{III}_{\text{hs}}$.

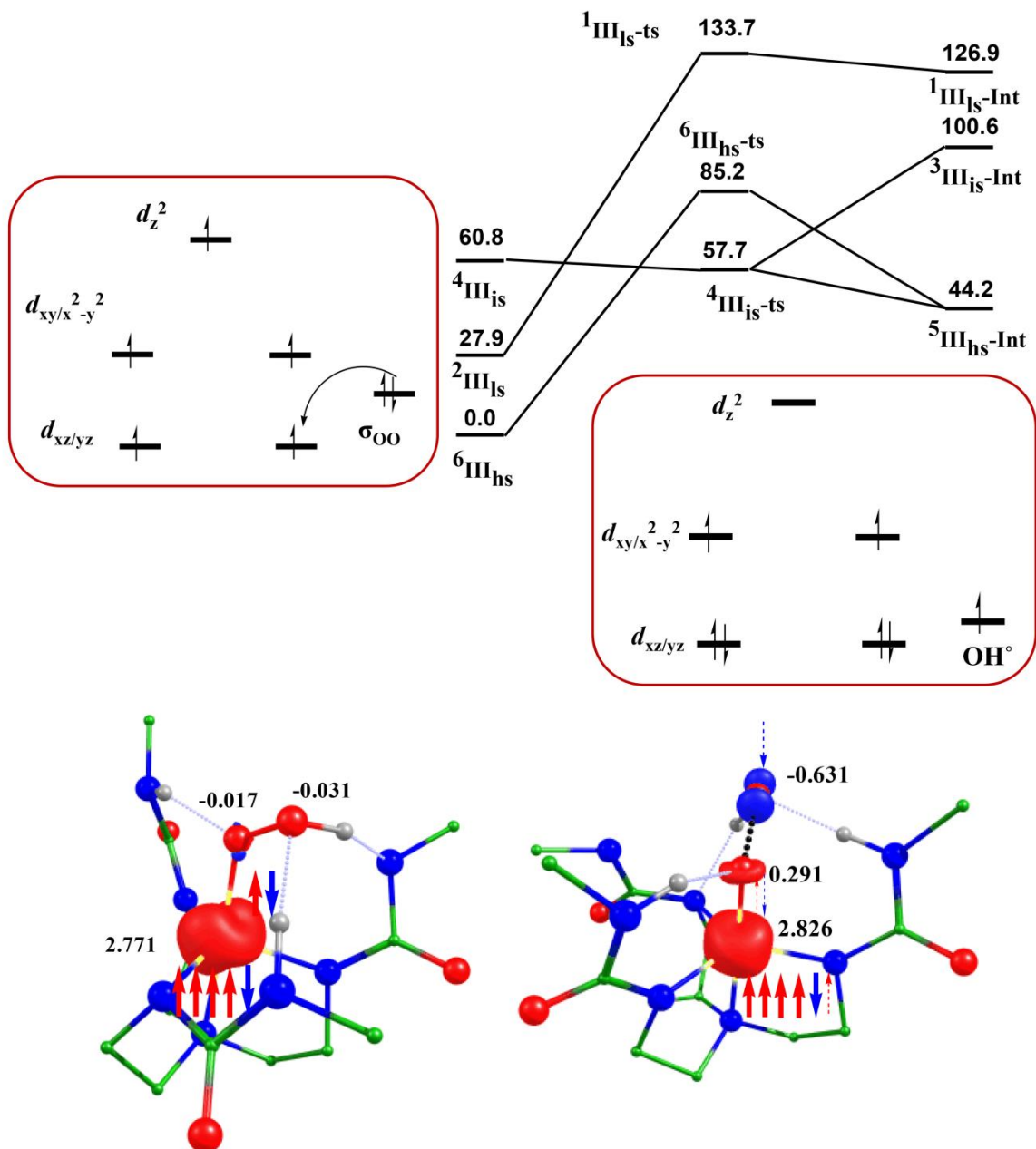


Fig. S10. B3LYP-D2 computed barrier height (ΔG in kJ mol⁻¹) along with schematic representation of electron involvement with spin density during the O-O bond cleavage of species III.

Similar to the chromium species there also exists the MCEP, because high spin surface (⁶III_{hs}) has the lowest energy while the ⁴III_{is-ts} have the lowest barrier for O---O bond cleavage thus MCEP exists between sextet and quartet spin surface.

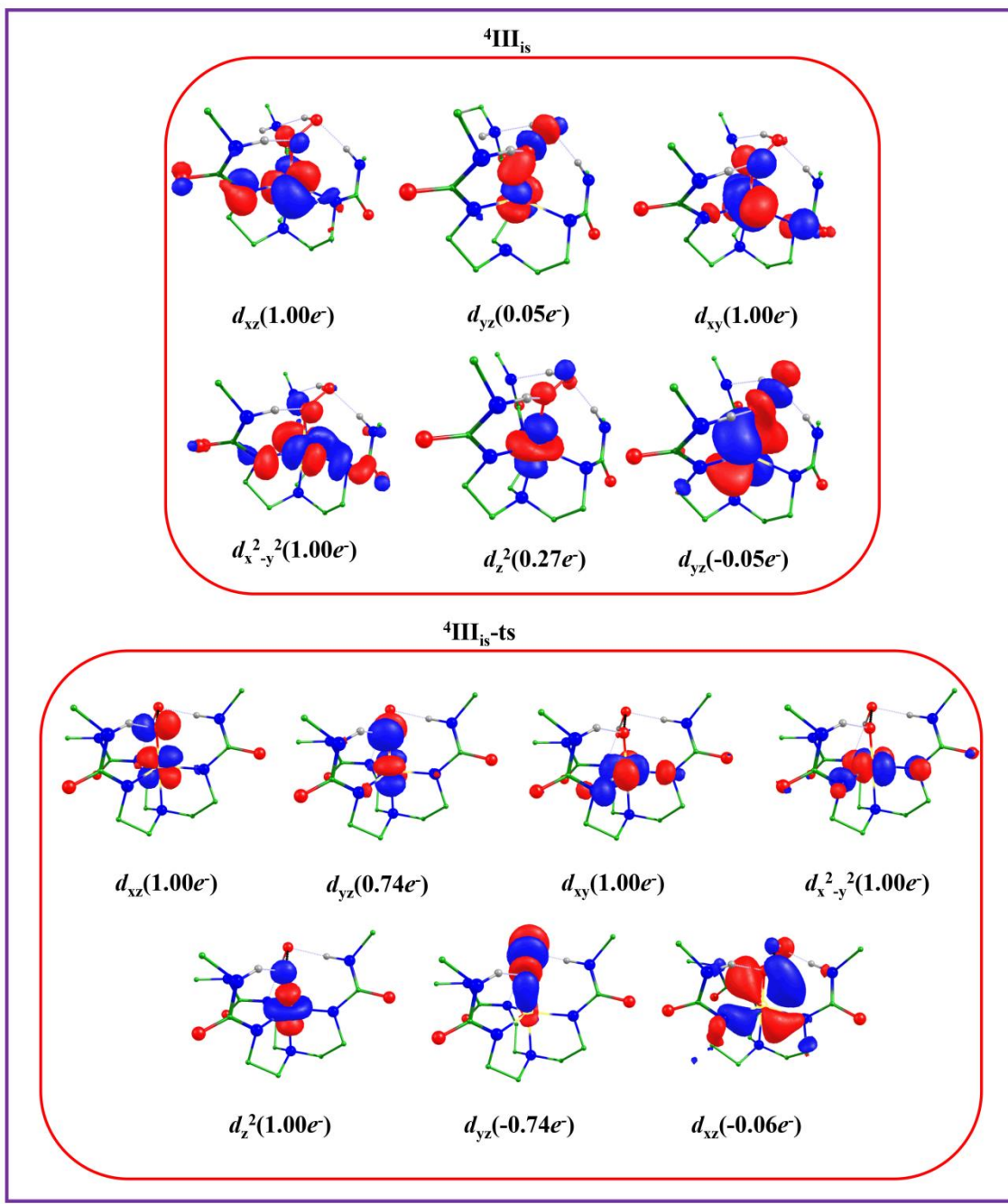


Fig. S11. Spin natural orbitals and their occupations (noted in parenthesis) of $^4\text{III}_{\text{is}}$ and $^4\text{III}_{\text{is-ts}}$.

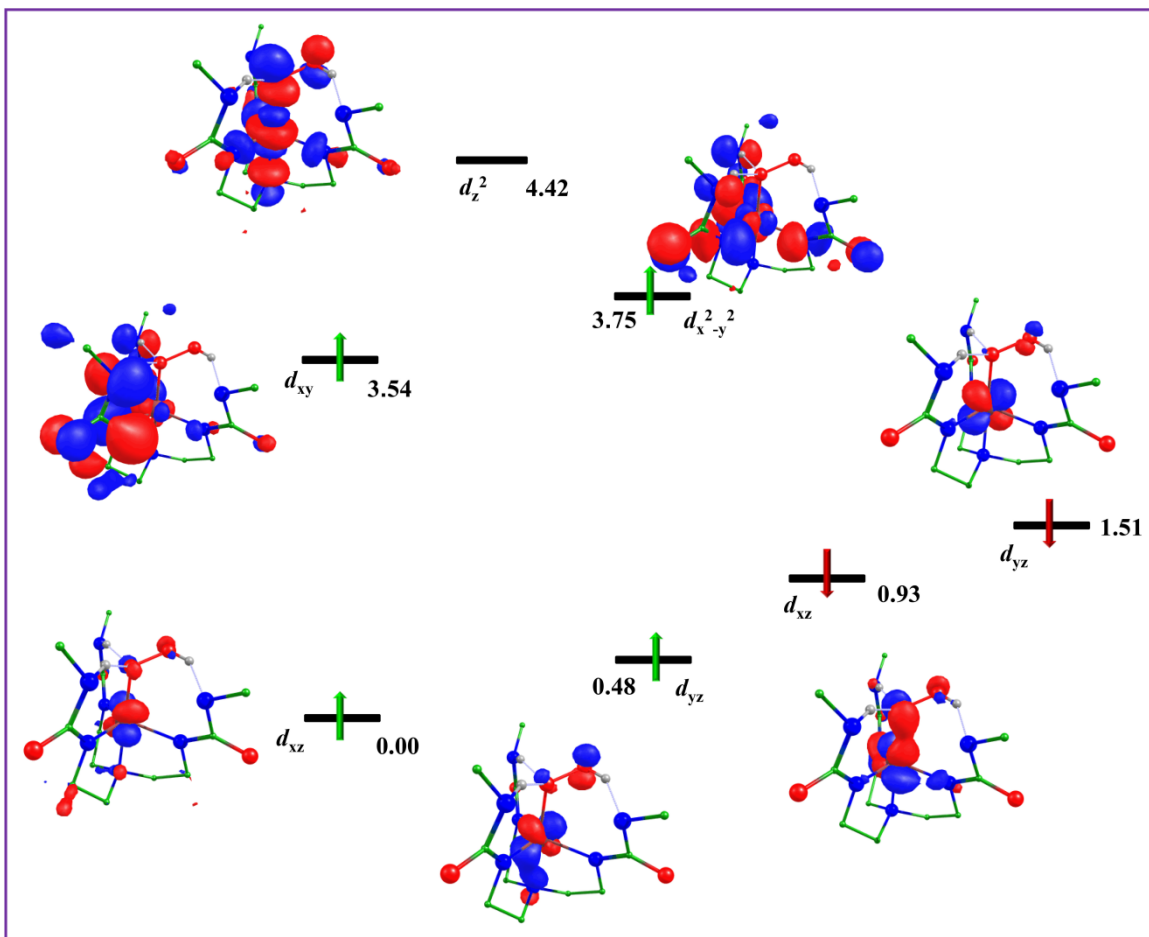


Fig. S12. Computed eigenvalue plot incorporating energies computed for d -based orbitals for alpha and beta spin corresponding to the ground state ${}^3\text{IV}_{\text{is}}$ of the species IV (energies are given in eV).

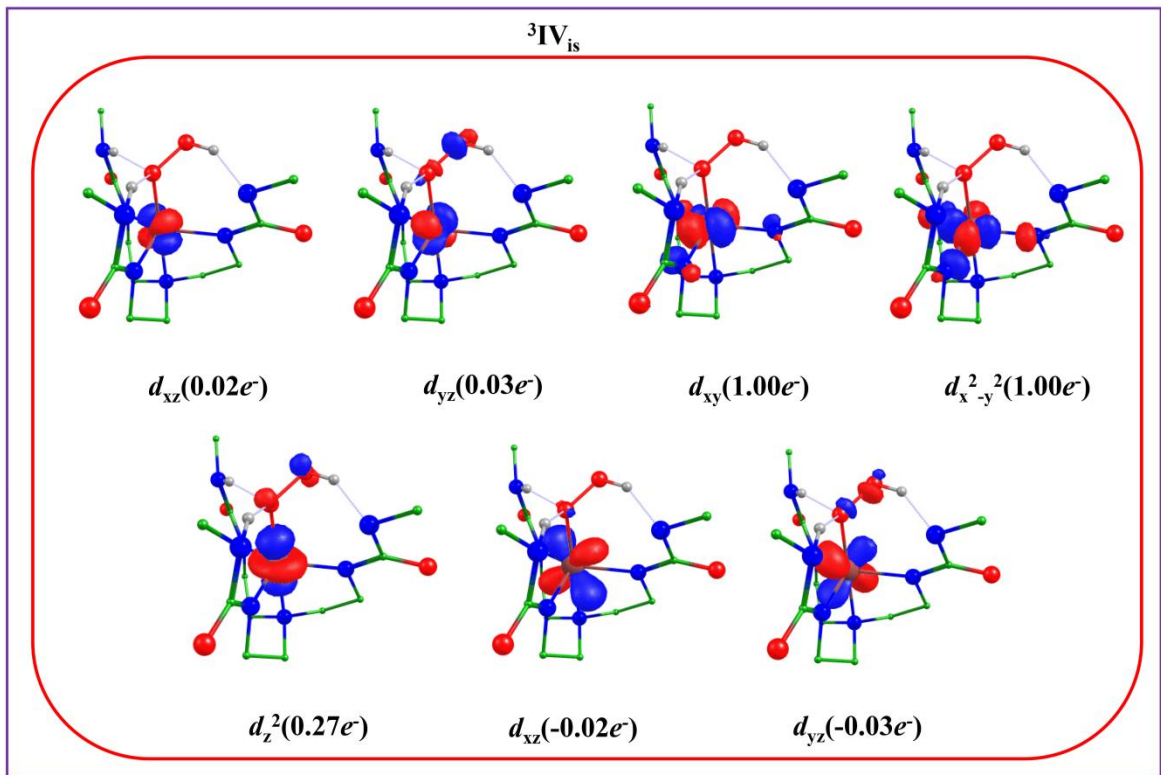


Fig. S13. Spin natural orbitals and their occupations (noted in parenthesis) of ${}^3\text{IV}_{\text{is}}$.

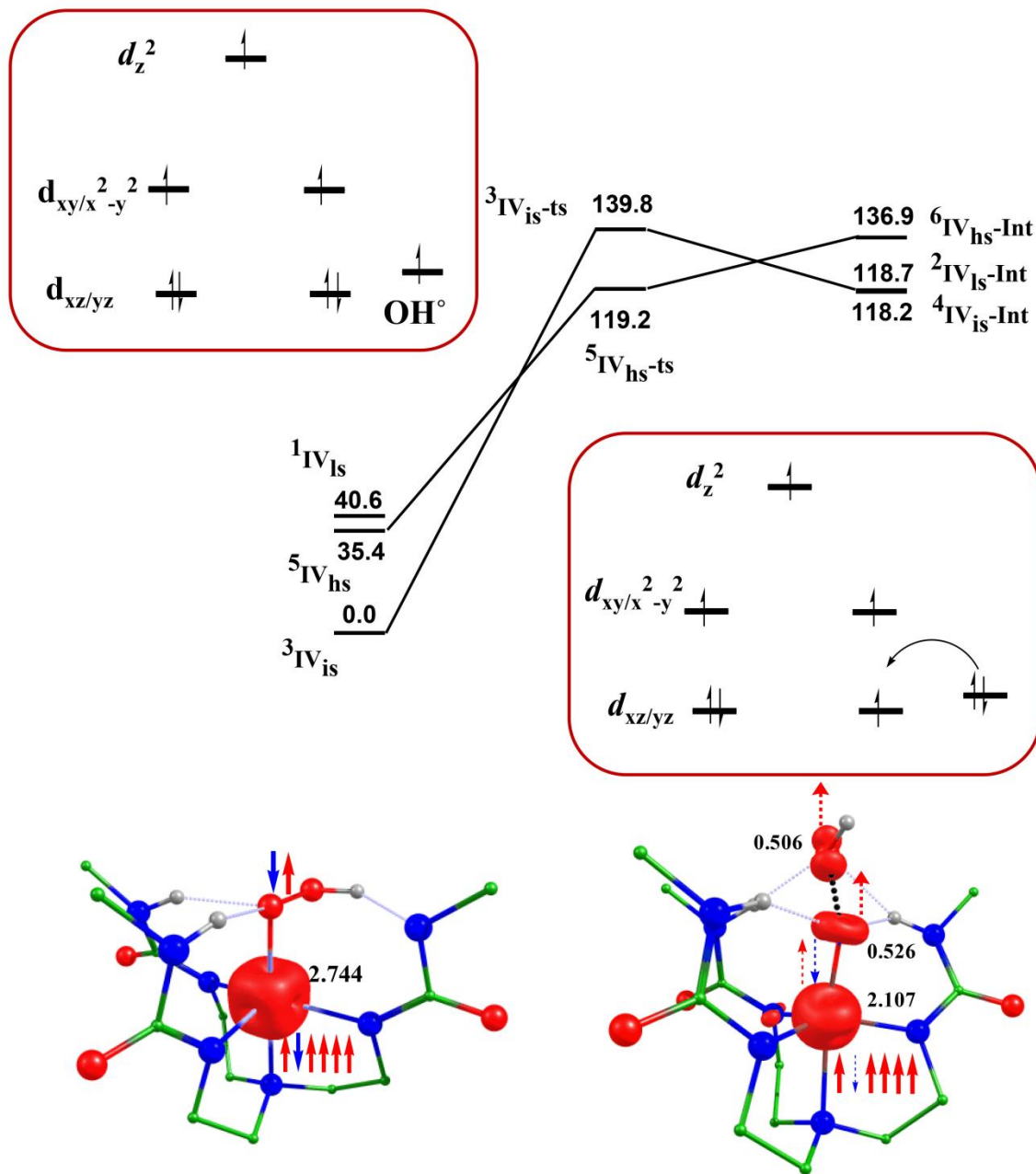


Fig. S14. B3LYP-D2 computed barrier height (ΔG in kJ mol^{-1}) along with schematic representation of electron involvement with spin density during the O--O bond cleavage of species IV.

Electron density at Co center is going to decrease from 2.744 (${}^5\text{IV}_{\text{hs}}$) to 2.107 indicates the formation of partial π bond between cobalt center and oxygen atom, where alpha electron from cobalt center and beta electron from bond pair of superoxo unit are involved. Here also MECP exist between ${}^3\text{IV}_{\text{is}}$ and ${}^5\text{IV}_{\text{hs-ts}}$.

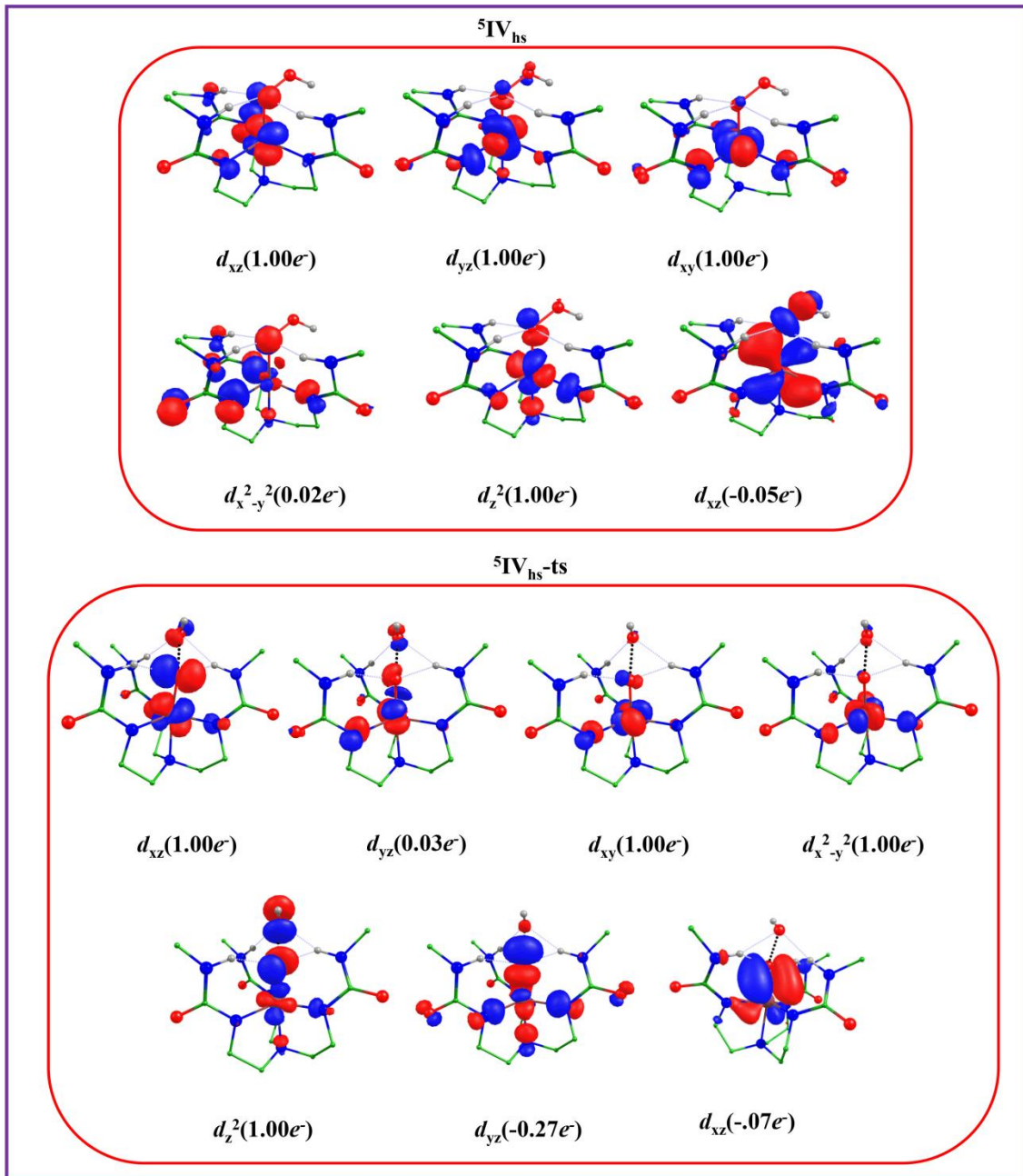


Fig. S15. Spin natural orbitals and their occupations (noted in parenthesis) of ${}^5\text{IV}_{\text{hs}}$ and ${}^5\text{IV}_{\text{hs-ts}}$.

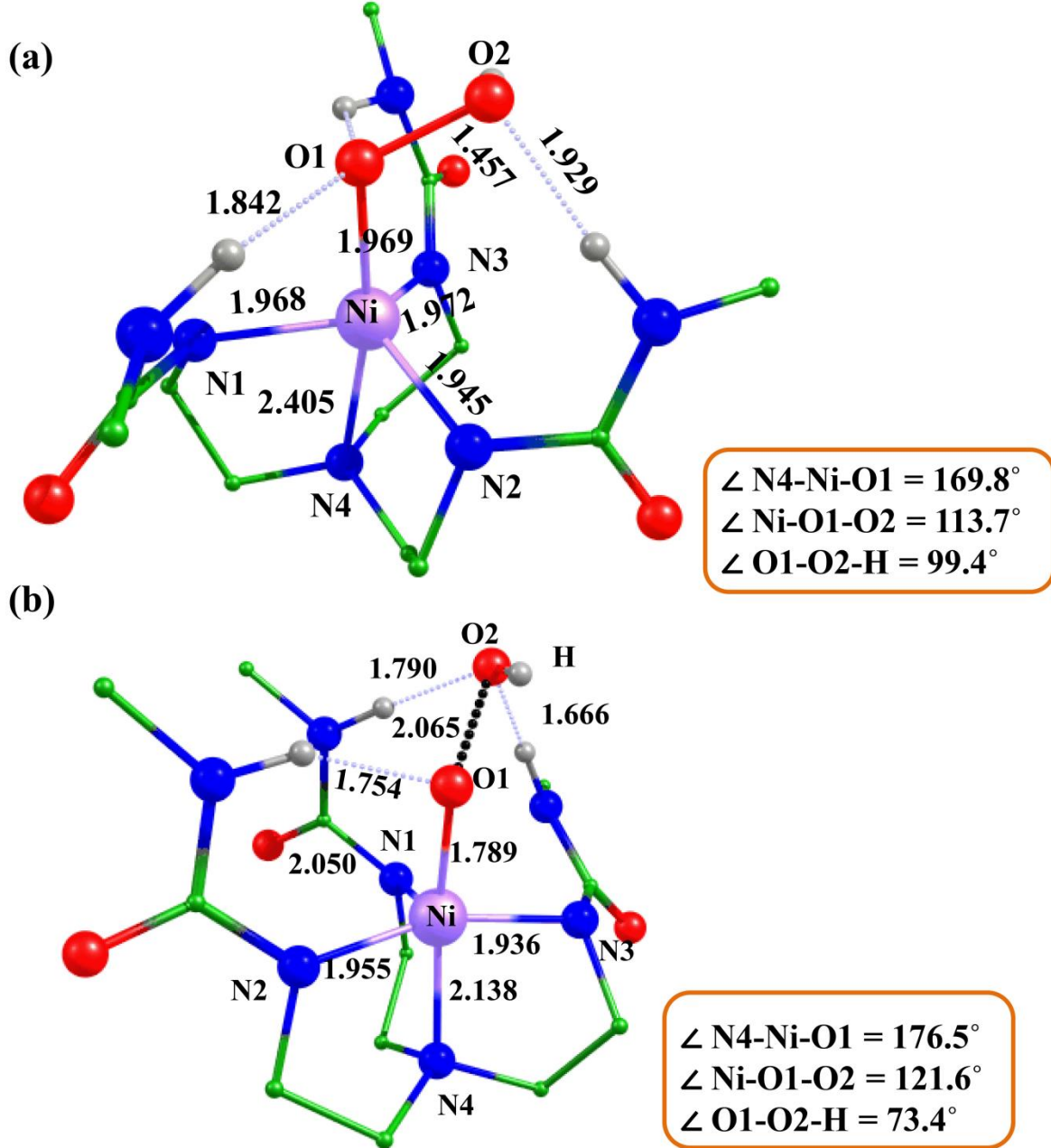


Fig. S16. B3LYP-D2 optimized structures of a) ${}^4\text{V}_{\text{hs}}$ and b) ${}^2\text{V}_{\text{ls-ts}}$ (bond lengths in Å).

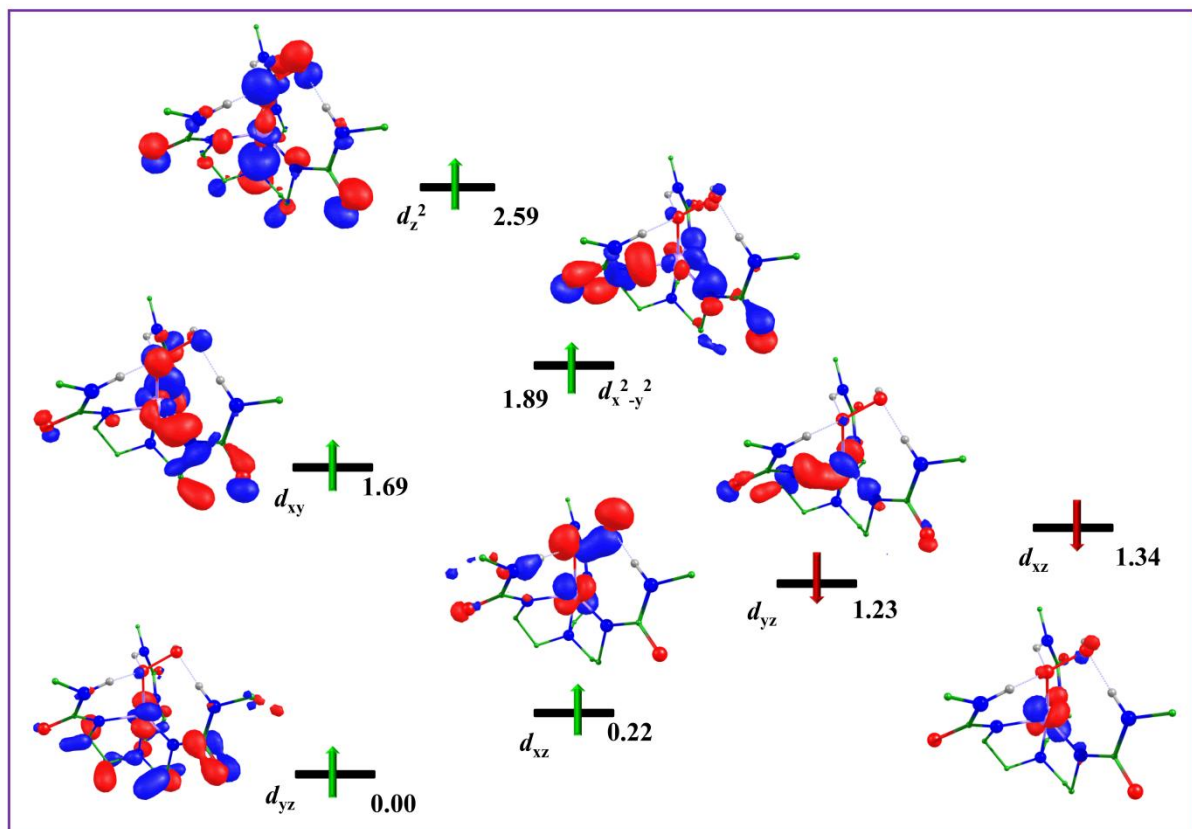


Fig. S17. Computed eigenvalue plot incorporating energies computed for *d*-based orbitals for alpha and beta spin corresponding to the ground state ${}^4V_{hs}$ of the species V (energies are given in eV).

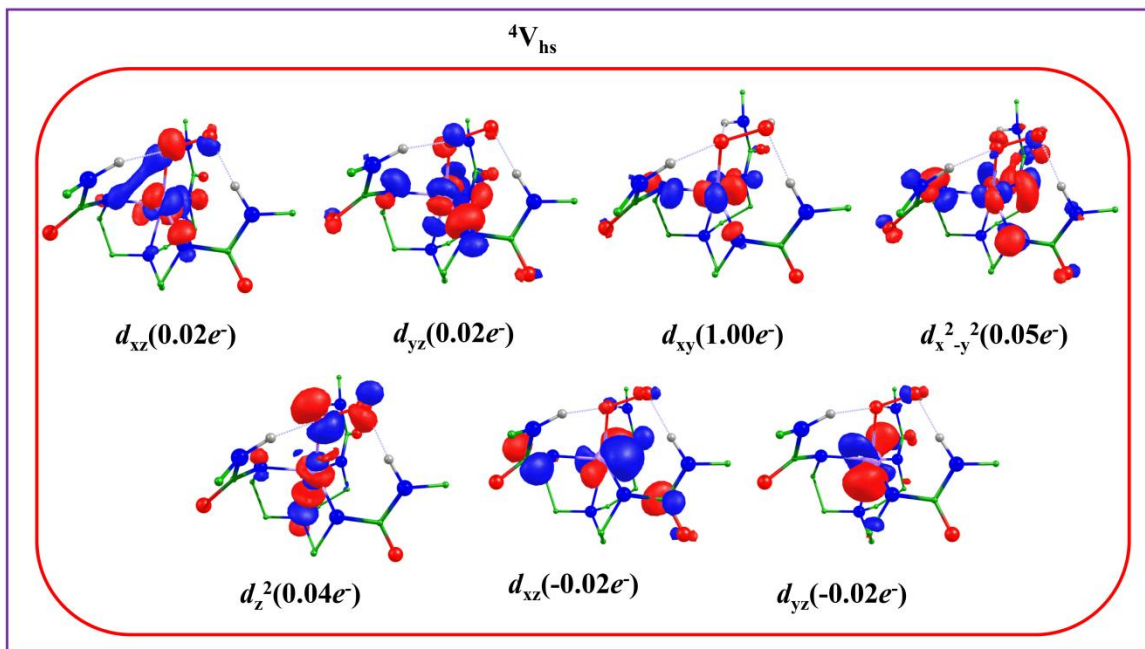


Fig. S18. Spin natural orbitals and their occupations (noted in parenthesis) of ${}^4V_{hs}$.

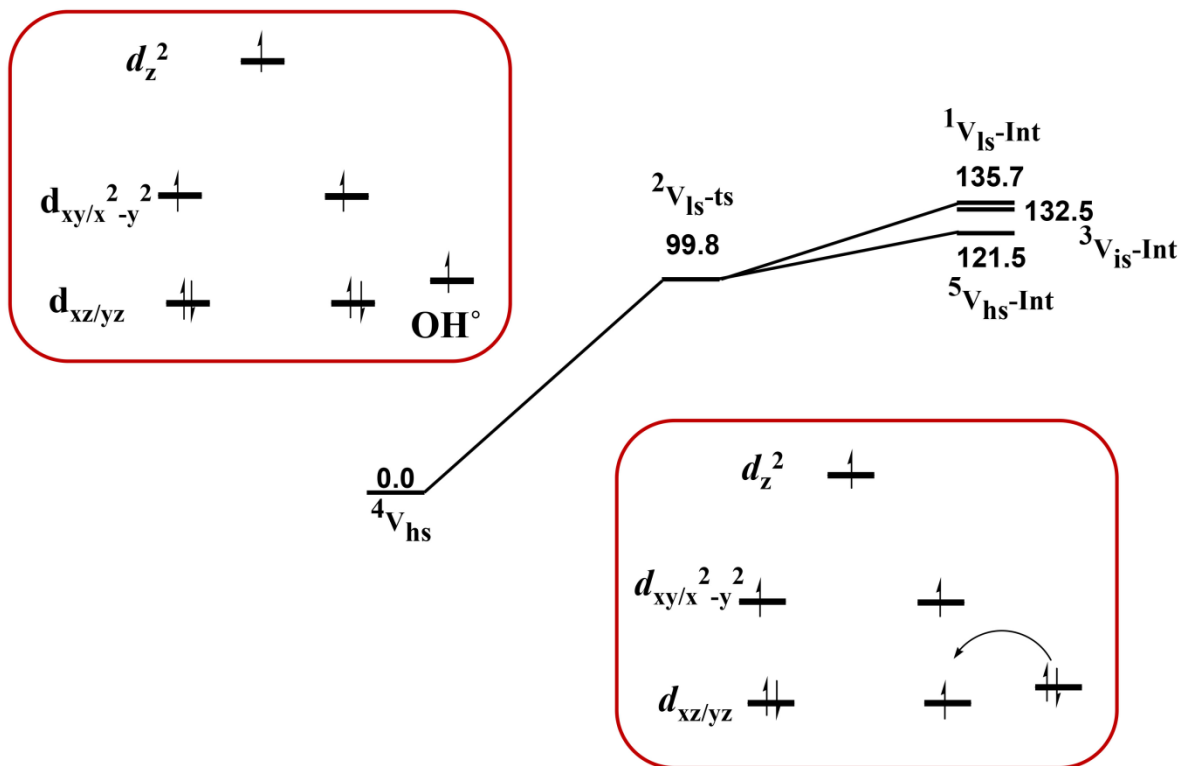


Fig. S19. B3LYP-D2 computed barrier height (ΔG in kJ mol^{-1}) of species V.

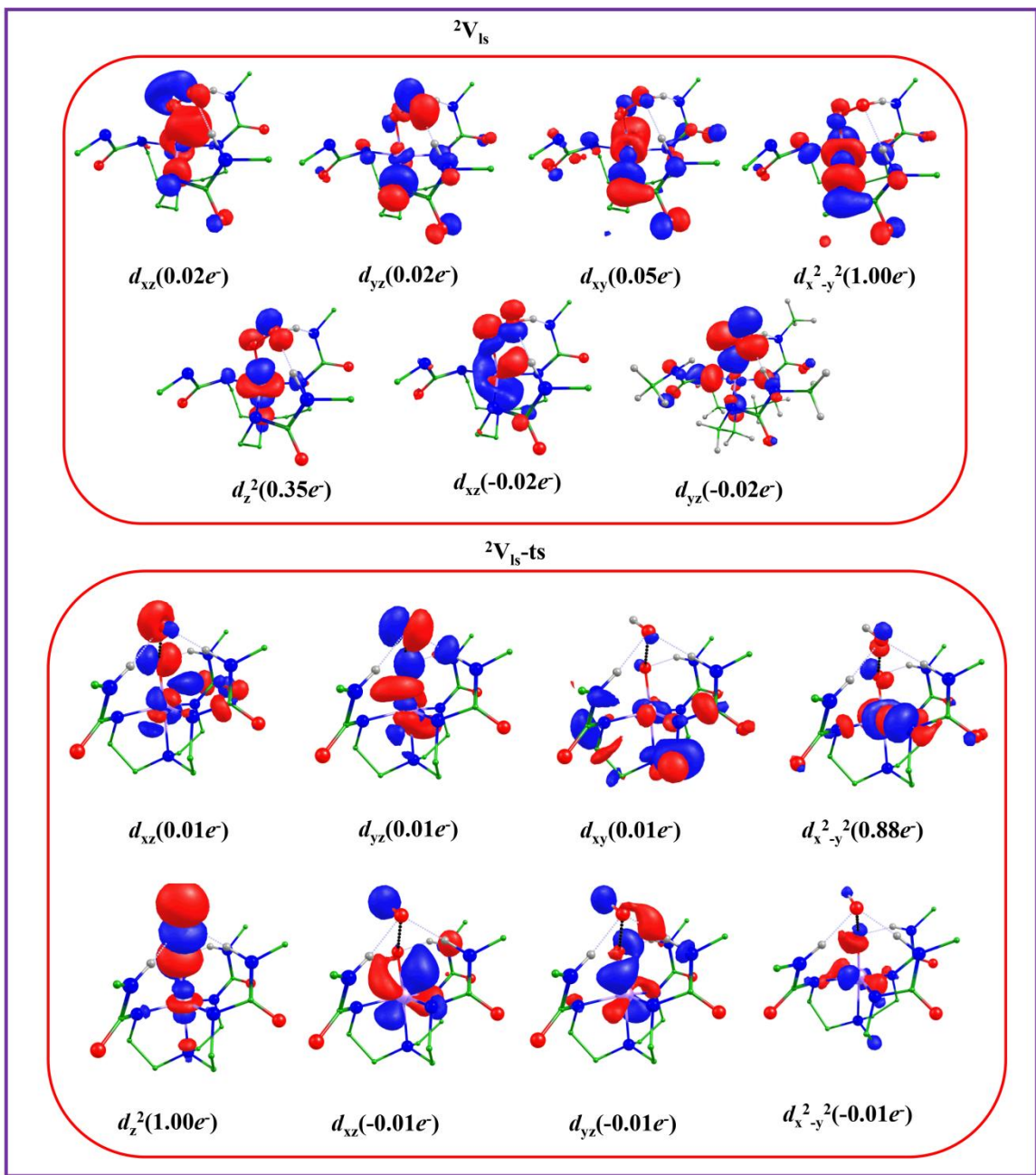


Fig. S20. Spin natural orbitals and their occupations (noted in parenthesis) of ${}^2V_{ls}$ and ${}^2V_{ls-ts}$.

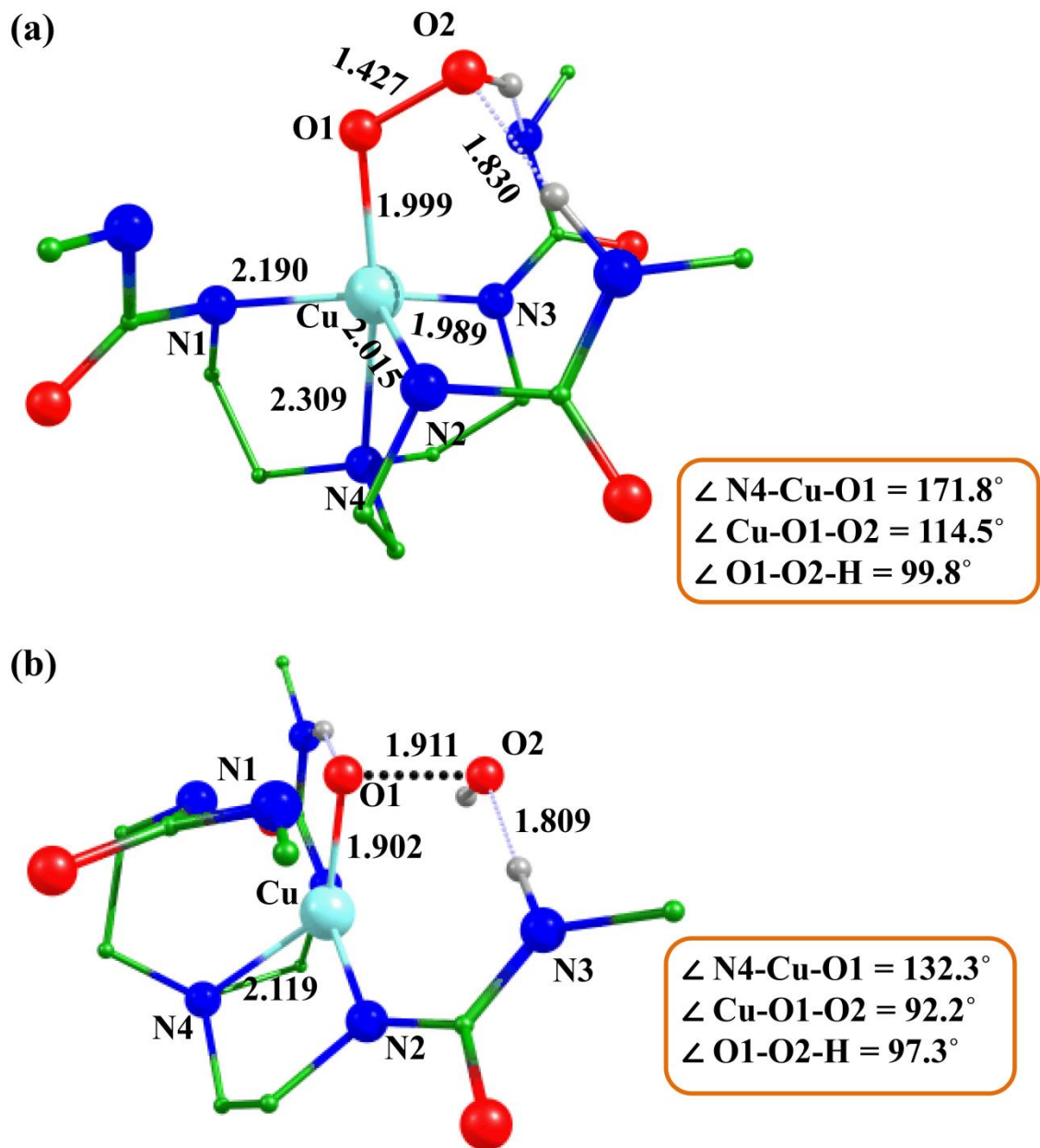


Fig. S21. B3LYP-D2 optimized structures of a) ${}^3\text{VI}_{\text{hs}}$ and b) ${}^1\text{VI}_{\text{ls-ts}}$ (bond lengths in Å).

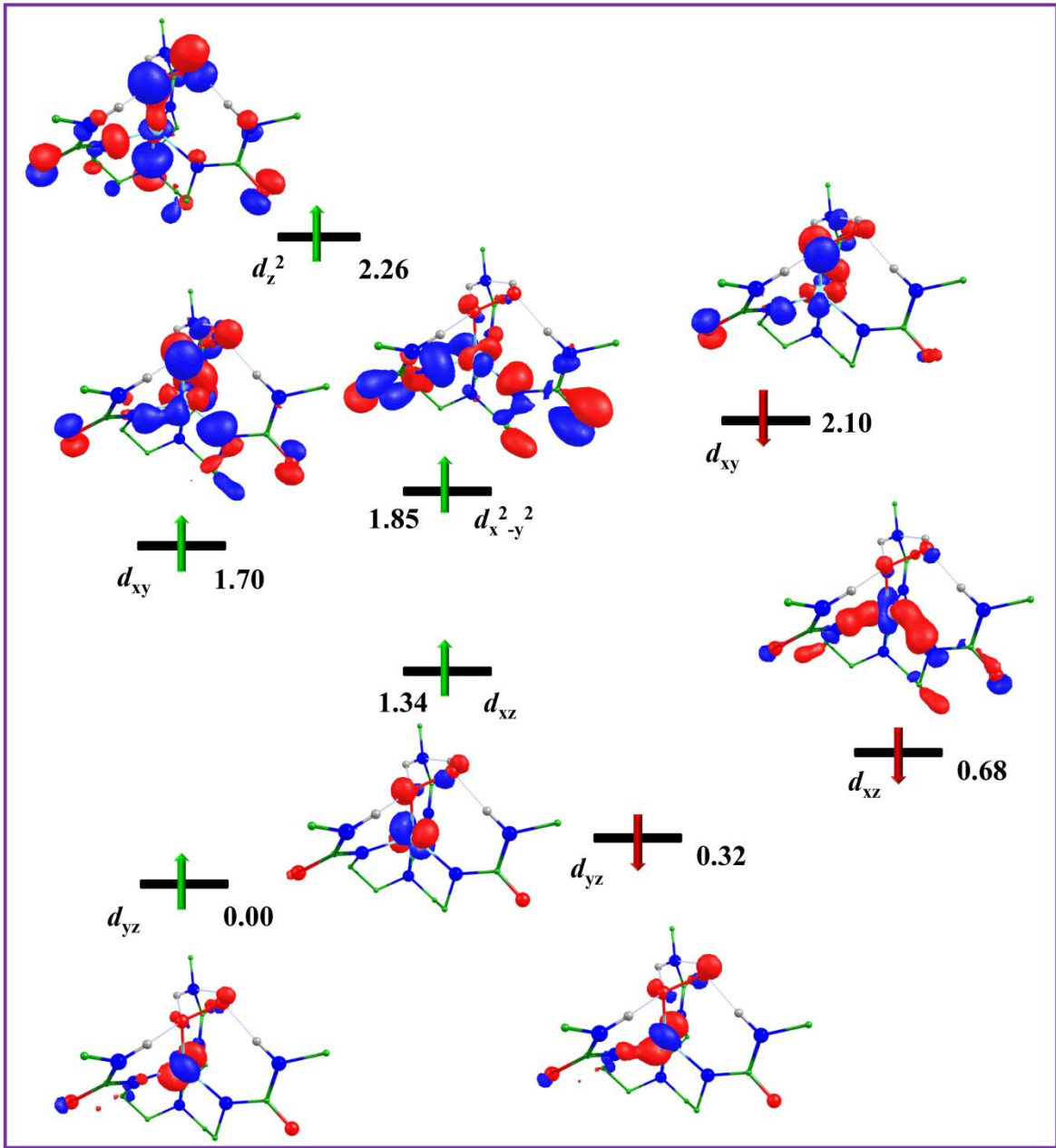


Fig. S22. Computed eigenvalue plot incorporating energies computed for d -based orbitals for alpha and beta spin corresponding to the ground state ${}^3\text{VI}_{\text{hs}}$ of the species VI (energies are given in eV).

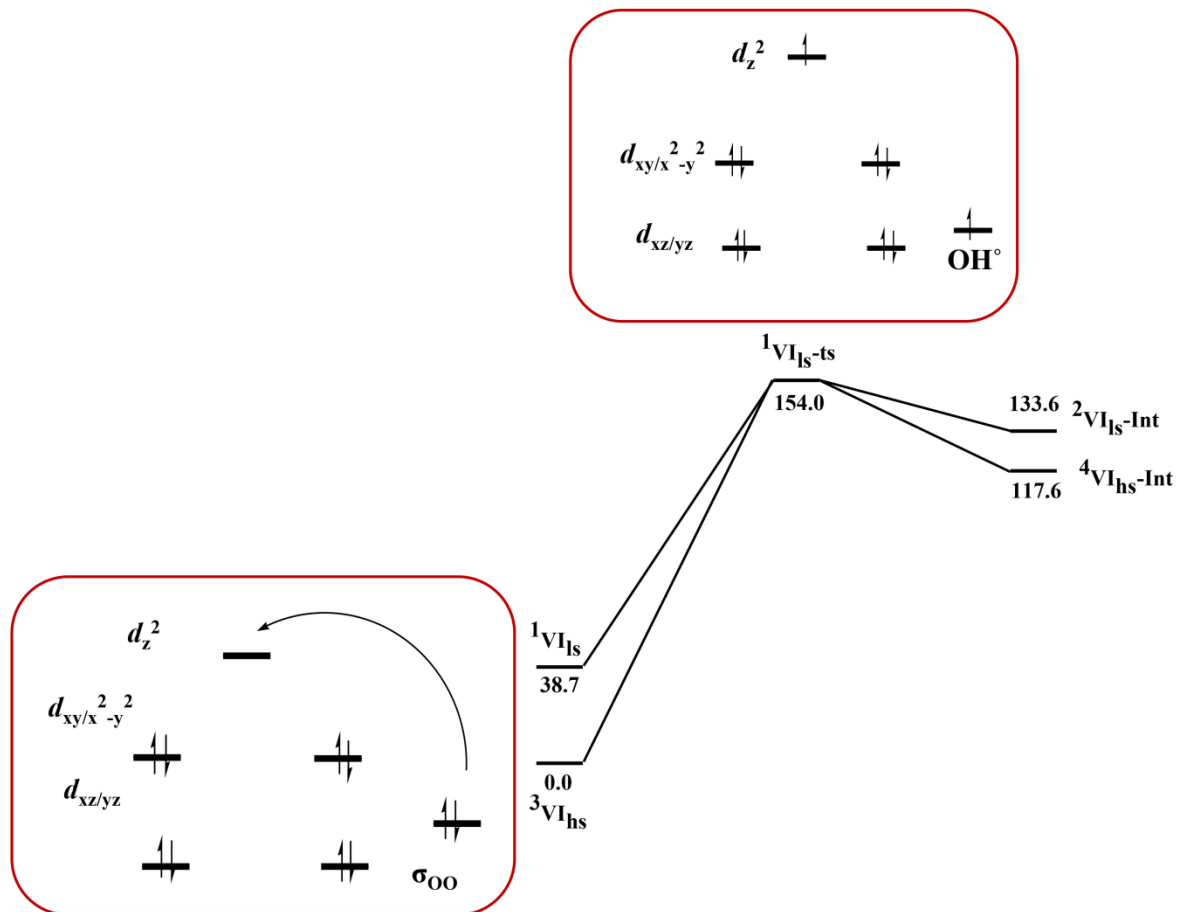


Fig. S23. B3LYP-D2 computed barrier height (ΔG in kJ mol⁻¹) species VI.

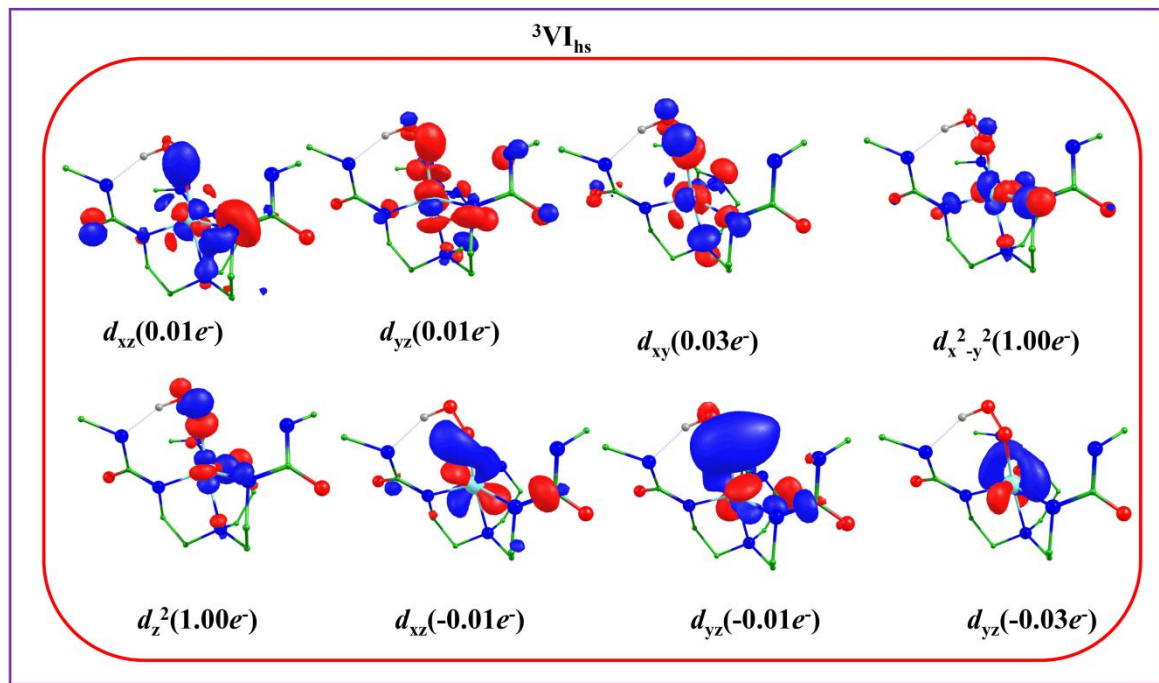
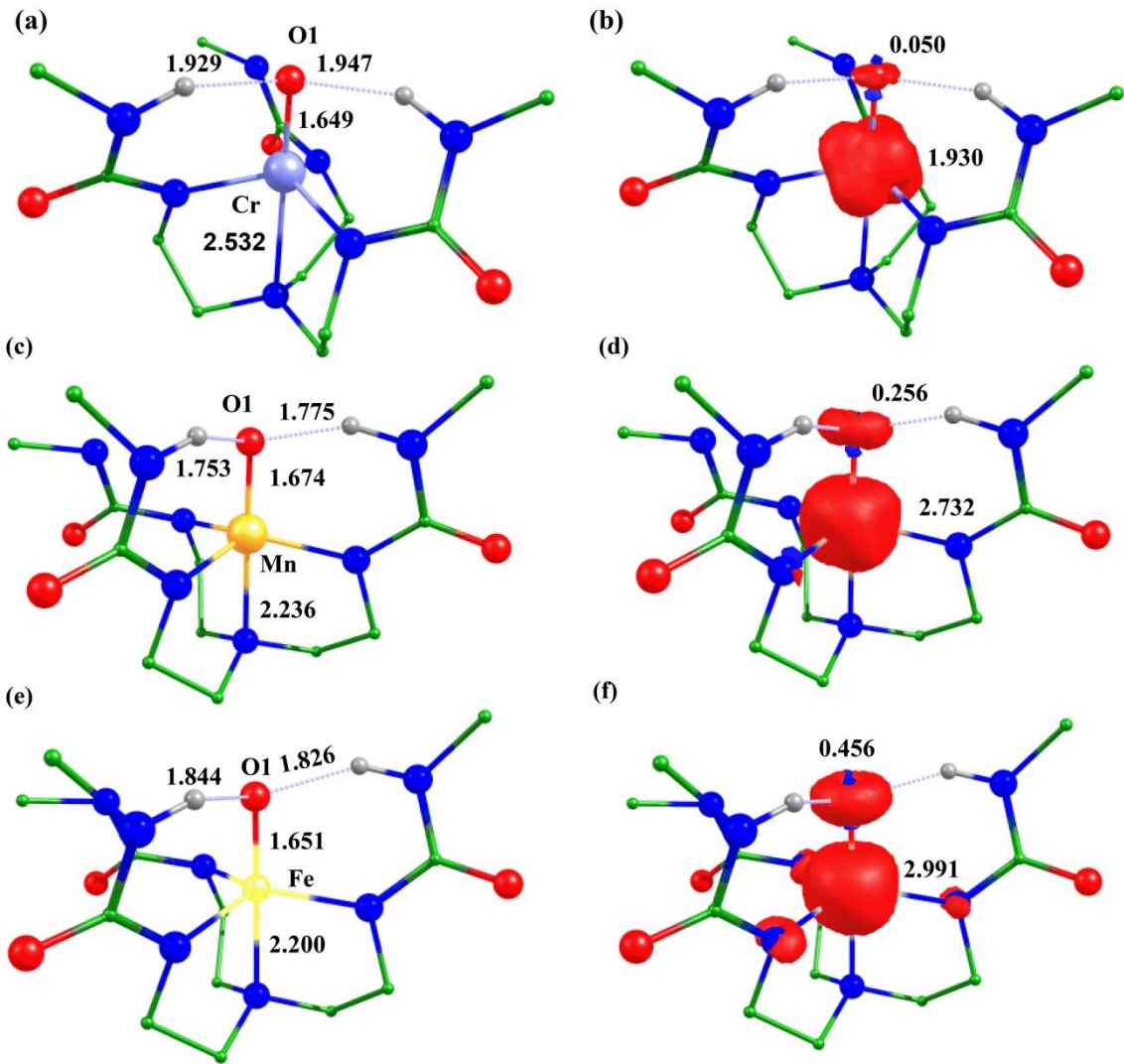


Fig. S24. Spin natural orbitals and their occupations (noted in parenthesis) of ${}^3\text{IV}_{\text{hs}}$.



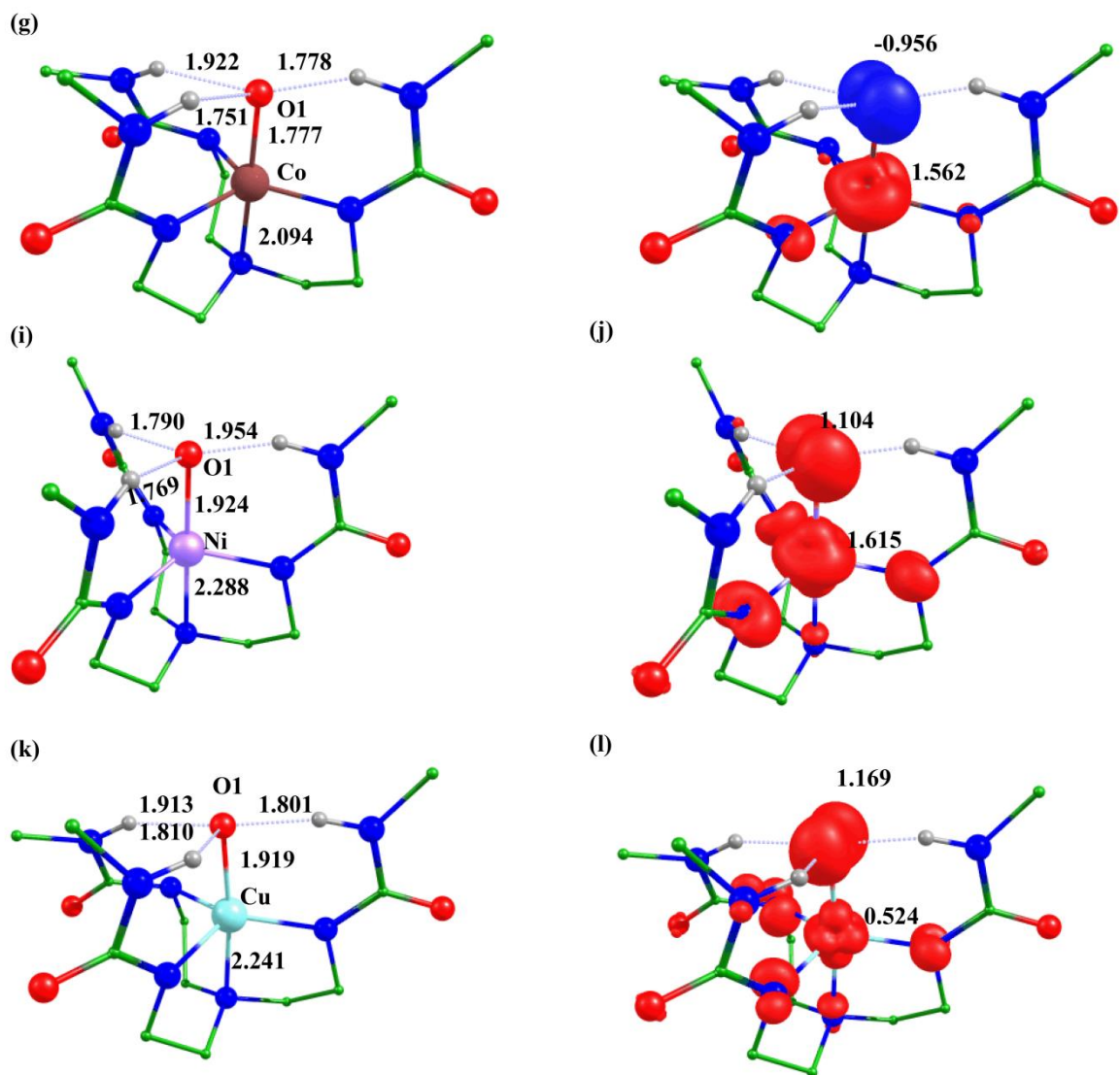


Fig. S25. B3LYP-D2 a) optimized structure of ${}^3\text{I}_{\text{hs}}$ -Int (bond lengths in Å) and b) its spin density plot; c) optimized structure of ${}^4\text{II}_{\text{hs}}$ -Int (bond lengths in Å) and d) its spin density plot; e) optimized structure of ${}^5\text{III}_{\text{hs}}$ -Int (bond lengths in Å) and f) its spin density plot; g) optimized structure of ${}^4\text{IV}_{\text{hs}}$ -Int (bond lengths in Å) and h) its spin density plot i) optimized structure of ${}^5\text{V}_{\text{hs}}$ -Int (bond lengths in Å) and j) its spin density plot; k) optimized structure of ${}^4\text{VI}_{\text{hs}}$ -Int (bond lengths in Å) and l) its spin density plot.

Table S5. B3LYP-D2 computed barrier height of O---O bond cleavage (in gaseous phase) of Ru, Os, Rh and Ir species with buea ligand.

Metal	Barrier height (in kJ/mol)
Ru (VII)	52.7
Os (VIII)	21.1
Rh (IX)	111.8
Ir (X)	77.3

Table S6. Selected B3LYP-D2 computed structural parameters of the buea metal-hydroperoxo species, transition states (O---O).

Spin State	Bond length (Å)										Bond Angle (°)					
	M-O	M-N ₁	M-N ₂	M-N ₃	M-N ₄	O-O	O-H ₁	O-H ₂	O-H ₃	O ₁ -M-N ₄	M-O1-O ₂	N ₁ -M-N ₂	N ₂ -M-N ₃	N ₁ -M-N ₃	N ₃ -M-N ₄	O-O-H
[(buea)RuOOH] ⁻ Species																
⁶ VII _{hs}	2.135	2.211	2.147	2.157	2.596	1.470	1.964	1.900	-	165.4	105.1	117.4	101.7	117.5	73.9	98.1
⁴ VII _{is}	1.960	2.108	2.209	2.094	2.239	1.465	1.928	1.770	1.897	174.0	115.3	103.5	145.6	98.3	79.5	100.9
² VII _{ls}	2.056	2.037	2.026	2.056	2.179	1.470	1.844	1.883	1.704	172.7	114.2	120.3	135.2	97.9	82.1	98.9
² VII _{hs-ts}	1.902	2.018	2.032	2.010	2.032	1.871	1.722	1.771	1.730	173.6	115.7	125.1	115.9	110.5	80.3	89.8
[(buea)OsOOH] ⁻ Species																
⁴ VIII _{is}	1.939	2.059	2.219	2.075	2.195	1.631	1.814	1.862	1.847	173.6	115.8	147.9	105.2	96.8	80.6	99.8
² VIII _{ls}	2.076	2.049	2.000	2.057	2.155	1.486	1.838	1.948	1.713	172.9	114.8	132.6	94.6	127.2	83.7	99.1
² VIII _{ls-ts}	1.960	2.001	2.038	2.042	2.193	1.762	1.689	1.715	1.754	171.3	121.1	122.2	126.2	104.4	80.6	92.4
[(buea)RhOOH] ⁻ Species																
⁵ IX _{hs}	2.121	2.149	2.155	2.124	2.481	1.444	1.963	1.865	-	172.5	100.2	128.6	111.3	102.1	77.3	100.2
³ IX _{is}	2.028	2.155	2.065	2.121	2.133	1.452	1.787	1.849	1.851	177.8	110.6	135.5	101.4	116.0	82.9	98.8
¹ IX _{ls}	2.007	2.073	2.018	2.109	2.154	1.447	-	1.738	1.895	176.6	103.5	157.5	93.9	99.3	82.9	98.9
³ IX _{is-ts}	1.891	1.909	2.067	2.088	2.067	2.214	1.722	1.819	-	173.2	116.2	127.5	123.1	102.2	81.5	90.6
[(buea)IrOOH] ⁻ Species																
⁵ X _{is}	2.135	2.144	2.132	2.143	2.533	1.460	1.983	1.950	-	173.4	117.9	110.9	125.4	105.5	75.4	100.0
³ X _{is}	2.063	2.069	2.038	2.194	2.112	1.470	1.993	1.849	-	178.0	111.6	143.7	104.3	106.4	80.7	99.2
¹ X _{ls}	2.071	2.104	1.996	2.085	2.102	1.468	1.726	1.794	1.892	178.7	134.2	136.2	84.2	134.2	84.6	99.4
¹ X _{ls-ts}	1.857	2.001	2.062	2.006	2.062	2.118	1.738	1.796	1.639	167.1	117.1	124.7	88.3	138.5	81.5	75.8

Table S7. Selected B3LYP-D2 computed spin density values of the buea species, transition states.

Spin State	M	O1	O2
[(buea)RuOOH] ⁻			
⁶ VII _{hs}	3.682	0.037	0.251
⁴ VII _{is}	2.283	0.135	0.005
² VII _{ls}	0.746	-0.002	-0.000
² VII _{ls} -ts	0.339	0.022	0.424
[(buea)OsOOH] ⁻			
⁴ VIII _{is}	2.304	0.182	0.007
² VIII _{ls}	0.773	0.005	-0.001
² VIII _{ls} -ts	0.507	0.020	0.245
[(buea)RhOOH] ⁻			
⁵ IX _{hs}	2.388	0.307	0.059
³ IX _{is}	1.268	-0.023	-0.000
¹ IX _{ls}	0	0	0
³ IX _{is} -ts	0.800	0.212	0.440
[(buea)IrOOH] ⁻			
⁵ X _{hs}	2.637	0.294	0.050
³ X _{is}	1.317	-0.007	0.008
¹ X _{ls}	0	0	0
¹ X _{ls} -ts	0	0	0

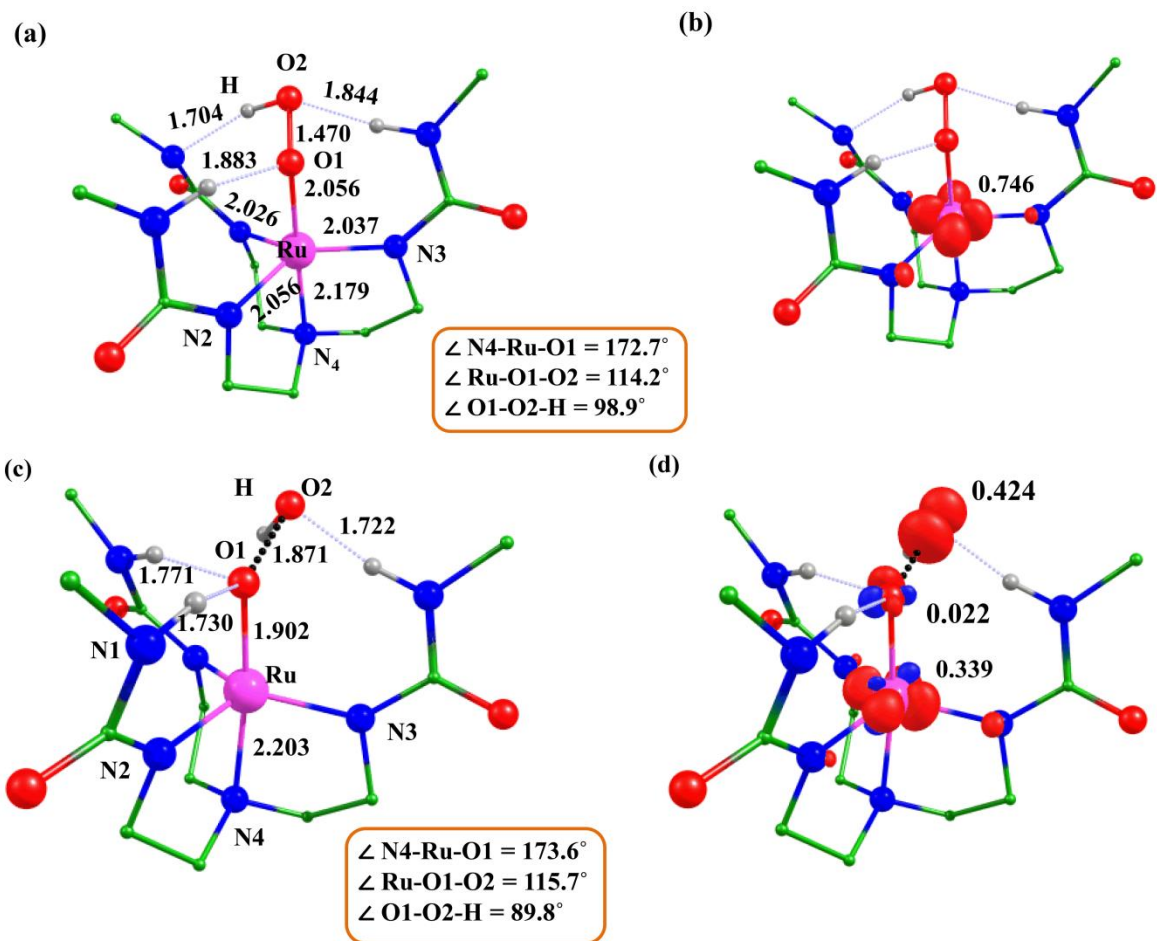


Fig. S26. B3LYP-D2 a) optimized structure of ${}^2\text{VII}_{\text{ls}}$ (bond lengths in Å) and b) its spin density plot, c) optimized structure of ${}^2\text{VII}_{\text{ls-ts}}$ (bond lengths in Å), and d) its spin density plot.

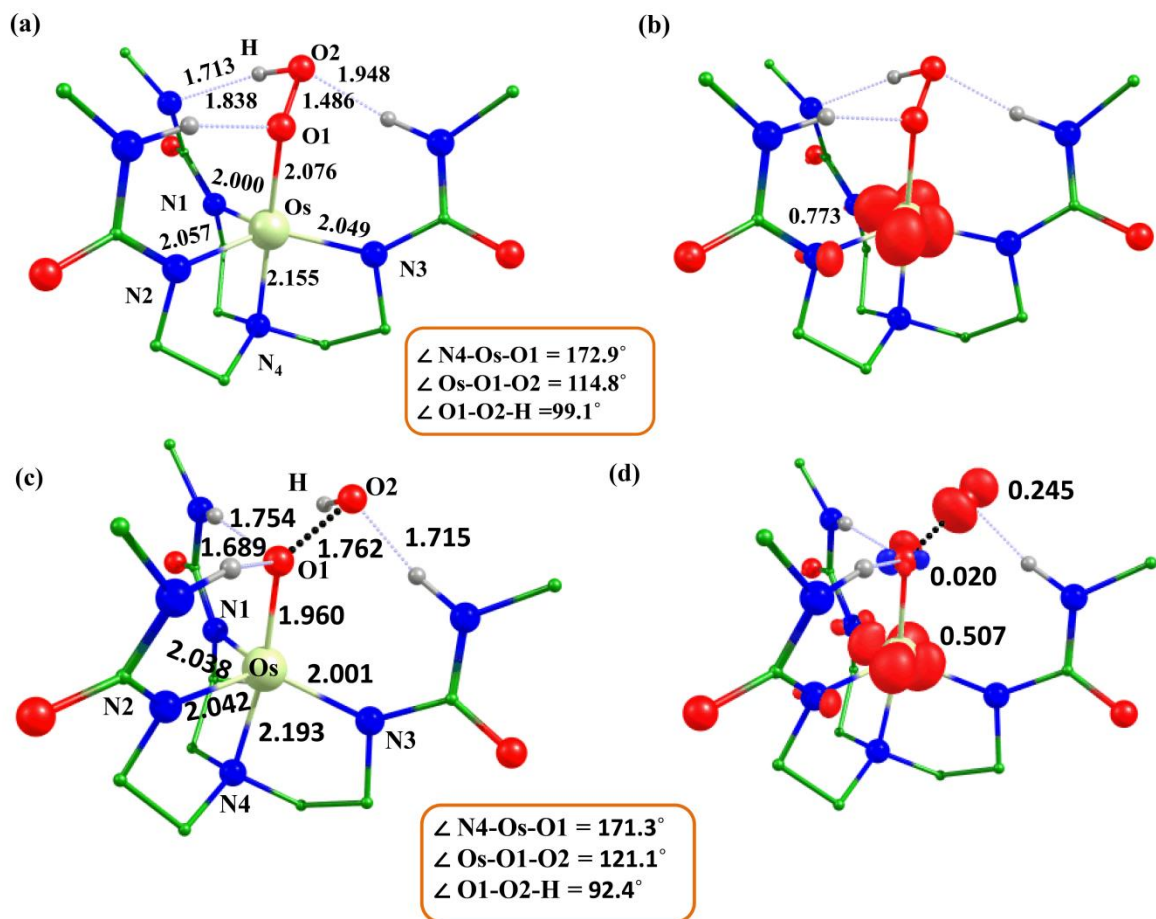


Fig. S27. B3LYP-D2 a) optimized structure of ${}^2\text{VIII}_{\text{ls}}$ (bond lengths in Å), and b) its spin density plot, c) optimized structure of ${}^2\text{VIII}_{\text{ls-ts}}$ (bond lengths in Å), and d) its spin density plot.

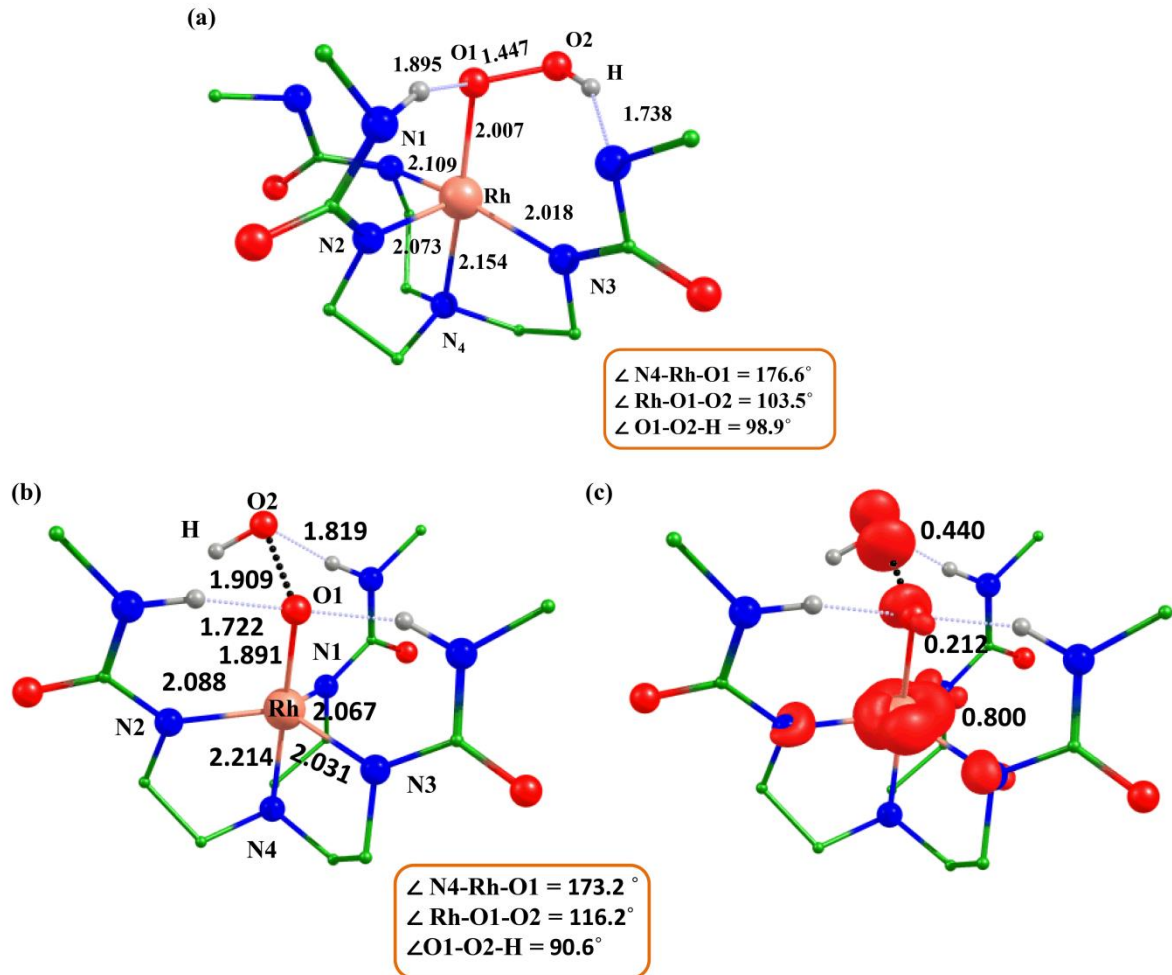


Fig. S28. B3LYP-D2 a) optimized structure of $^1\text{IX}_{\text{ls}}$ (bond length in Å), b) optimized structure of $^3\text{IX}_{\text{ts}}$ -ts (bond lengths in Å) and c) its spin density plot.

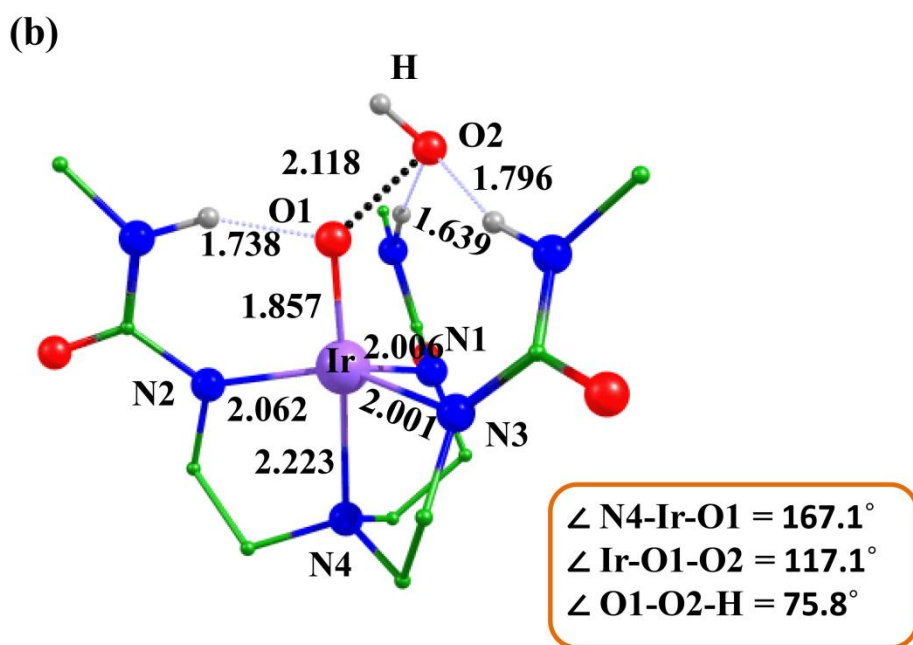
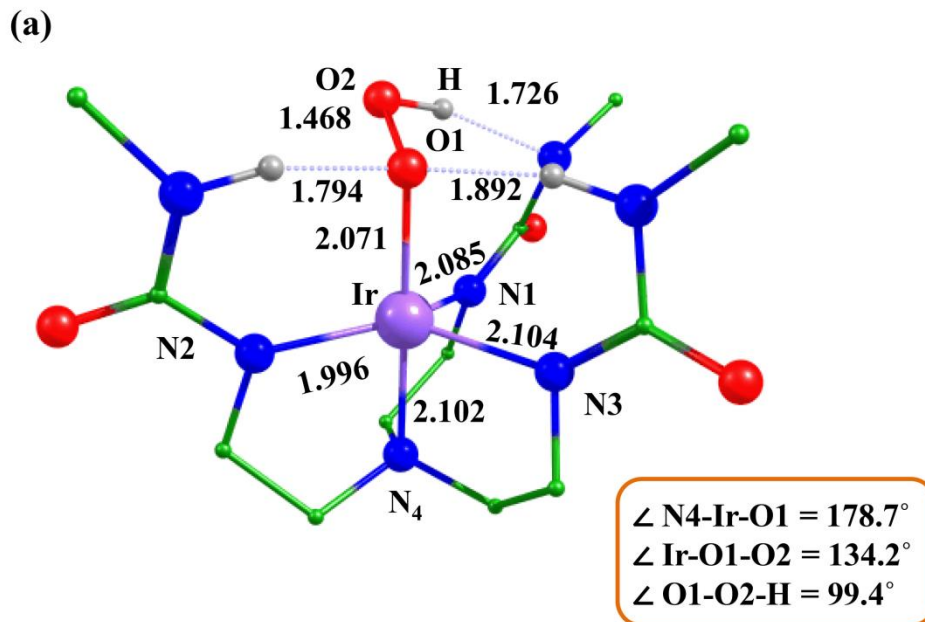


Fig. S29. B3LYP-D2 a) optimized structures of ${}^1\text{X}_{\text{l}\text{s}}$ and b) ${}^1\text{X}_{\text{l}\text{s}-\text{ts}}$ (bond lengths in Å).

Table S8. Computed stretching frequencies of M-O bond in metal-oxo species.

Metal-oxo	ν (cm ⁻¹)
³ I _{hs} -Int	921
⁴ II _{hs} -Int	851
⁵ III _{hs} -Int	889
⁴ IV _{is} -Int	515
⁵ V _{hs} -Int	390
⁴ VI _{hs} -Int	419

References

1. M. J. Frisch, G. W. Trucks, H. B. Schlegel, G. E. Scuseria, M. A. Robb, J. R. Cheeseman, G. Scalmani, V. Barone, B. Mennucci, G. A. Petersson, H. Nakatsuji, M. Caricato, X. Li, H. P. Hratchian, A. F. Izmaylov, J. Bloino, G. Zheng, J. L. Sonnenberg, M. Hada, M. Ehara, K. Toyota, R. Fukuda, J. Hasegawa, M. Ishida, T. Nakajima, Y. Honda, O. Kitao, H. Nakai, T. Vreven, J. A. Montgomery Jr., J. E. Peralta, F. Ogliaro, M. Bearpark, J. J. Heyd, E. Brothers, K. N. Kudin, V. N. Staroverov, R. Kobayashi, J. Normand, K. Raghavachari, A. Rendell, J. C. Burant, S. S. Iyengar, J. Tomasi, M. Cossi, N. Rega, J. M. Millam, M. Klene, J. E. Knox, J. B. Cross, V. Bakken, C. Adamo, J. Jaramillo, R. Gomperts, R. E. Stratmann, O. Yazyev, A. J. Austin, R. Cammi, C. Pomelli, J. W. Ochterski, R. L. Martin, K. Morokuma, V. G. Zakrzewski, G. A. Voth, P. Salvador, J. J. Dannenberg, S. Dapprich, A. D. Daniels, Ö. Farkas, J. B. Foresman, J. V. Ortiz, J. Cioslowski and D. J. Fox, Gaussian, Inc., Wallingford, CT, 2016.
2. (a) A. D. Becke, *J. Chem. Phys.*, 1993, **98**, 5648-5652; (b) C. Lee, W. Yang and R. G. Parr, *Phys. Rev. B: Condens. Matter Mater. Phys.*, 1988, **37**, 785-789.
3. S. J. Grimme, *Comput. Chem.*, 2006, **27**, 1787-1799.
4. J. D. Chai and M. Head-Gordon, *Phys. Chem. Chem. Phys.*, 2008, **10**, 6615-6620.
5. (a) A. Ansari, A. Kaushik and G. Rajaraman, *J. Am. Chem. Soc.*, 2013, **135**, 4235-4249; (b) A. Ansari and G. Rajaraman, *Phys. Chem. Chem. Phys.*, 2014, **16**, 14601-14613; (c) K. P. Kepp, *J. Inorg. Biochem.*, 2011, **105**, 1286-1292; (d) Monika and A. Ansari, *New J. Chem.* 2020, **44**, 19103-19112.
6. (a) A. Ansari, M. Ansari, A. Singha and G. Rajaraman, *Chem. Eur. J.*, 2017, **23**, 10110-10125; (b) A. Ansari, P. Jayapal and G. Rajaraman, *Angew. Chem. Int. Ed.*, 2015, **127**, 564-568; (c) R. Kumar, A. Ansari and G. Rajaraman, *Chem. Eur. J.*, 2018, **24**, 6660-6860.
7. (a) T. H. Dunning Jr. and P. J. Hay, *In Modern Theoretical Chemistry* (Ed: Schaefer, H. F.), Plenum, New York, 1976; Vol. 3; (b) P. J. Hay and W. R. Wadt, *J. Chem. Phys.*, 1985, **82**, 270-283; (c) P. J. Hay and W. R. Wadt, *J. Chem. Phys.*, 1985, **82**, 299-310.

8. M. M. Franci, W. J. Pietro, W. J. Hehre, J. S. Binkley, M. S. Gordon, D. J. DeFrees, J. A. Pople, *J. Chem. Phys.* 1982, **77**, 3654-3665.
9. (a) A. Schaefer, H. Horn and R. Ahlrichs, *J. Chem. Phys.*, 1992, **97**, 2571-2577; (b) C. Schaefer, C. Huber and R. Ahlrichs, *Chem. Phys.*, 1994, **100**, 5829-5835.
10. J. Cho, J. Woo and W. Nam, *J. Am. Chem. Soc.* 2010, **132**, 5958-5959.
11. S. Hong, H. So, H. Yoon, K.-B. Cho, Y.-M. Lee, S. Fukuzumi and W. Nam, *Dalton Trans.*, 2013, **42**, 7842-7845.
12. J. Cho, H. Y. Kang, L. V. Liu, R. Sarangi, E. I. Solomon and W. Nam, *Chem. Sci.*, 2013, **4**, 1502-1508.
13. A. Ansari, P. Jayapal and G. Rajaraman, *Angew. Chem., Int. Ed.*, 2015, **127**, 574-578.
14. J. Cho, R. Sarangi and W. Nam, *Acc. Chem. Res.*, 2012, **45**, 1321-1330.
15. J.-U. Rohde, J.-H. In, M. H. Lim, W. W. Brennessel, M. R. Bukowski, A. Stubna, E. Munck, W. Nam and L. Que, Jr., *Science*, 2003, **299**, 1037-1039.
16. R. L. Halbach, D. Gygi, E. D. Bloch, B. L. Anderson and D. G. Nocera, *Chem. Sci.*, 2018, **9**, 4524-4528.